

---

# Average gradient outer product as a mechanism for deep neural collapse

---

Daniel Beaglehole<sup>\*,1</sup> Peter Súkeník<sup>\*,2</sup> Marco Mondelli<sup>2</sup> Mikhail Belkin<sup>1</sup>

<sup>1</sup>UC San Diego <sup>2</sup>Institute of Science and Technology Austria

## Abstract

Deep Neural Collapse (DNC) refers to the surprisingly rigid structure of the data representations in the final layers of Deep Neural Networks (DNNs). Though the phenomenon has been measured in a variety of settings, its emergence is typically explained via data-agnostic approaches, such as the unconstrained features model. In this work, we introduce a data-dependent setting where DNC forms due to feature learning through the average gradient outer product (AGOP). The AGOP is defined with respect to a learned predictor and is equal to the uncentered covariance matrix of its input-output gradients averaged over the training dataset. Deep Recursive Feature Machines are a method that constructs a neural network by iteratively mapping the data with the AGOP and applying an untrained random feature map. We demonstrate theoretically and empirically that DNC occurs in Deep Recursive Feature Machines as a consequence of the projection with the AGOP matrix computed at each layer. We then provide evidence that this mechanism holds for neural networks more generally. We show that the right singular vectors and values of the weights can be responsible for the majority of within-class variability collapse for DNNs trained in the feature learning regime. As observed in recent work, this singular structure is highly correlated with that of the AGOP.

## 1 Introduction

How Deep Neural Networks (DNNs) learn a transformation of the data to form a prediction and what are the properties of this transformation constitute fundamental questions in the theory of deep learning. A promising avenue to understand the hidden mechanisms of DNNs is Neural Collapse (NC) [Papayan et al., 2020]. NC is a widely observed structural property of overparametrized DNNs, occurring in the terminal phase of gradient descent training on classification tasks. This property is linked with the performance of DNNs, such as generalization and robustness [Papayan et al., 2020, Su et al., 2023]. NC is defined by four properties that describe the geometry of feature representations of the training data in the last layer. Of these, in this paper we focus on the following two, because they are relevant in the context of deeper layers. The *within-class variability collapse* (NC1) states that feature vectors of the training samples within a single class collapse to the common class-mean. The *orthogonality or simplex equiangular tight frame property* (NC2) states that these class-means form an orthogonal or simplex equiangular tight frame. While initially observed in just the final hidden layer, these properties were measured for the intermediate layers of DNNs as well [Rangamani et al., 2023, He and Su, 2022], indicating that NC progresses depth-wise. This has led to the definition and study of the Deep Neural Collapse (DNC), a direct depth-wise extension of the standard Neural Collapse [Súkeník et al., 2023].

The theoretical explanations of the formation of (D)NC have mostly relied on a data-agnostic model, known as *unconstrained features model* (UFM) [Mixon et al., 2020, Lu and Steinerberger, 2022].

---

<sup>\*</sup>Equal contribution. Correspondence to: Daniel Beaglehole (dbeaglehole@ucsd.edu), Peter Súkeník (peter.sukenik@ista.ac.at).

This assumes that DNNs are infinitely expressive and, thus, optimizes for the feature vectors in the last layer directly. The deep UFM (DUFM) was then introduced to account for more layers [Súkeník et al., 2023, Tirer and Bruna, 2022]. The (D)UFM has been identified as a useful analogy for neural network collapse, as (D)NC emerges naturally in this setting for a variety of loss functions and training regimes (see Section 2). However, (D)UFM discards the training data and most of the network completely, thus ignoring also the role of feature learning in DNC. This is a serious gap to fully understand the formation of DNC in the context of the full DNN pipeline.

In this paper, we introduce a setting where DNC forms that is highly dependent on the training data and predictor - iterated linear mapping onto the average gradient outer product (AGOP). The AGOP is the uncentered covariance matrix of the input-output gradients of a predictor averaged over its training data. Recent work has utilized this object to understand various surprising phenomena in neural networks including grokking, lottery tickets, simplicity bias, and adversarial examples [Radhakrishnan et al., 2024a]. Additional work incorporated layer-wise linear transformation with the AGOP into kernel machines, to model the deep feature learning mechanism of neural networks [Beaglehole et al., 2023]. The output of their backpropagation-free method, Deep Recursive Feature Machines (Deep RFM), is a standard neural network at i.i.d. initialization, where each random weight matrix is additionally right-multiplied by the AGOP of a kernel machine trained on the input to that layer. Their method was shown to improve performance of convolutional kernels on vision datasets and recreate the edge detection ability of convolutional neural networks.

Strikingly, we show that the neural network generated by this very same method, Deep RFM, exhibits deep neural collapse (Section 4). We establish in this setting that projection onto the AGOP is responsible for DNC in Deep RFM both empirically and theoretically. We verify these claims with an extensive experimental evaluation, which demonstrates a consistent formation of DNC in Deep RFM across several vision datasets. We then provide a theoretical analysis that explains this mechanism in the asymptotic high-dimensional regime and the smaller data regime under additional assumptions. The first analysis is based on the approximate linearity of kernel matrices when the dimension and the number of data points are large. We argue in our second analysis that the formation of DNC in Deep RFM is optimal in the kernel ridge regression sense.

We then give substantial evidence that projection onto the AGOP is linked to DNC formation in standard DNNs. In particular, we show that within-class variability collapse for DNNs can be primarily caused by the application of the right singular vectors of the weight matrix and the subsequent multiplication with its singular values (Section 5). Indeed, if  $W$  were unitary, then the common metric of within-class variability for  $X$  (the neural representations that are multiplied by  $W$ ) and  $WX$  are equal. Thus, the only way in which the application of a linear layer reduces the within-class variability is by erasing the within-class differences via the small singular directions of  $W$ . This operation can be viewed as discarding irrelevant information, or denoising.

The small singular directions of  $W$  are defined by its right singular vectors and singular values. Therefore, it is fully deducible from the Gram matrix of the weights at each layer,  $W^\top W$ . Radhakrishnan et al. [2024a], Beaglehole et al. [2023] have identified that, in many settings and across all layers of the network,  $W^\top W$  is approximately proportional to the average gradient outer product (AGOP) with respect to the inputs to that layer, in a statement termed the *Neural Feature Ansatz* (NFA). The NFA suggests that neural networks extract features from the data representations at every layer by projection onto the AGOP with respect to that layer.

Our results demonstrate that (i) AGOP is a mechanism for DNC in Deep RFM, and (ii) when the NFA holds, i.e. with small initialization, the right singular structure of  $W$ , and therefore the AGOP, induces the majority of within-class variability collapse in DNNs. We thus establish projection onto the AGOP as a setting for DNC formation that incorporates the data through feature learning.

## 2 Related work

**Neural collapse (NC).** Since the seminal paper by Pappas et al. [2020], the phenomenon of neural collapse has attracted significant attention. Galanti et al. [2022] use NC to improve generalization bounds for transfer learning, while Wang et al. [2023] discuss transferability capabilities of pre-trained models based on their NC on the target distribution. Haas et al. [2022] argue that NC can lead to improved OOD detection. Connections between robustness and NC are discussed in Su et al. [2023]. For a survey, we refer the interested reader to Kothapalli [2023].

The main theoretical framework to study the NC is the Unconstrained Features Model (UFM) [Mixon et al., 2020, Lu and Steinerberger, 2022]. Under this framework, many works have shown the emergence of the NC, either via optimality and/or loss landscape analysis [Weinan and Wojtowysch, 2022, Lu and Steinerberger, 2022, Zhou et al., 2022], or via the study of gradient-based optimization [Ji et al., 2022, Han et al., 2022, Wang et al., 2022]. Some papers also focus on the generalized class-imbalanced setting, where the NC does not emerge in its original formulation [Thrampoulidis et al., 2022, Fang et al., 2021, Hong and Ling, 2023]. Deviating from the strong assumptions of the UFM model, a line of work focuses on gradient descent in homogeneous networks [Poggio and Liao, 2020, Xu et al., 2023, Kunin et al., 2022], while others introduce perturbations [Tirer et al., 2022].

**AGOP feature learning.** The NFA was shown to capture many aspects of feature learning in neural networks including improved performance and interesting structural properties. The initial work on the NFA connects it to the emergence of spurious features and simplicity bias, why pruning DNNs may increase performance, the “lottery ticket hypothesis”, and a mechanism for grokking in vision settings [Radhakrishnan et al., 2024a]. Zhu et al. [2023] connect large learning rates and catapults in neural network training to better alignment of the AGOP with the true features. Radhakrishnan et al. [2024b] demonstrate that the AGOP recovers the implicit bias of deep linear networks toward low-rank solutions in matrix completion. Beaglehole et al. [2024] identify that the NFA is characterized by alignment of the weights to the pre-activation tangent kernel.

### 3 Preliminaries

#### 3.1 Notation

For simplicity, we assume a class-balanced setting, where  $N = Kn$  is the total number of training samples, with  $K$  being the number of classes and  $n$  the number of samples per class. Let us order the training samples such that the labels  $Y \in \mathbb{R}^{K \times N}$  can be written as  $I_K \otimes \mathbf{1}_n^\top$ , where  $I_K$  denotes a  $K \times K$  identity matrix,  $\otimes$  denotes the Kronecker product and  $\mathbf{1}_n$  a row vector of all-ones of length  $n$ . For a matrix  $A$  and a column vector  $v$ , the operation  $A \oplus v$ , divides each row of  $A$  by the corresponding element of  $v$ .

Both a DNN and Deep RFM of depth  $L$  can be written as:

$$f(x) = W_{L+1} \sigma(m_L \sigma(m_{L-1} \dots \sigma(m_1(x)) \dots)),$$

where  $m_l$  is an affine map and  $\sigma$  is a non-linear activation function. If the matrix  $m_l$  is defined by a single matrix, as in fully-connected networks, and not a product, we denote it by a weight matrix  $W_l$ . Each weight matrix is decomposed via its SVD as  $W_l = U_l S_l V_l^\top$ . The training data  $X_1 \in \mathbb{R}^{d_1 \times N}$  is stacked into columns and we let  $X_l, \tilde{X}_l, l \geq 2$  be the feature representations of the training data after  $l$  layers of the DNN after and before the non-linearity, respectively.

#### 3.2 Deep Neural Collapse

We define the feature vectors  $x_{ci}^l$  of the  $i$ -th sample of the  $c$ -th class as the input to  $m_l$ . Then,  $\tilde{x}_{ci}^l$  are the feature vectors produced from  $m_{l-1}$  before the application of  $\sigma$ , and are defined only for  $l > 1$ . Let  $\mu_c^l := \frac{1}{n} \sum_{i=1}^n x_{ci}^l$ ,  $\tilde{\mu}_c^l := \frac{1}{n} \sum_{i=1}^n \tilde{x}_{ci}^l$  be the corresponding class means, and  $H_l, \tilde{H}_l \in \mathbb{R}^{d_l \times K}$  the matrices of class means. We will also consider the centered and normalized class means  $\bar{H}_l = (H_l - \mu_G^l) \oplus (H_l - \mu_G^l)$ , where  $\mu_G^l$  is the global feature mean at layer  $l$ . NC1 is defined in terms of the *within-class* and *between-class* variability at layer  $l$ :

$$\Sigma_W^l = \frac{1}{N} \sum_{c=1}^K \sum_{i=1}^n (x_{ci}^l - \mu_c^l)(x_{ci}^l - \mu_c^l)^\top, \quad \Sigma_B^l = \frac{1}{K} \sum_{c=1}^K (\mu_c^l - \mu_G^l)(\mu_c^l - \mu_G^l)^\top.$$

**Definition 3.1.** In the context of this work, the neural collapse at layer  $l$  is achieved if the following two properties are satisfied:

- **DNC1:** The within-class variability at layer  $l$  is 0. This property can be stated for the features either after or before the application of the activation function  $\sigma$ . In the former case, the condition requires  $x_{ci}^l = x_{cj}^l$  for all  $i, j \in \{1, \dots, n\} \triangleq [n]$  (or, in matrix notation,  $X_l = H_l \otimes \mathbf{1}_n^\top$ ); in the latter,  $\tilde{x}_{ci}^l = \tilde{x}_{cj}^l$  for all  $i, j \in [n]$  (or, in matrix notation,  $\tilde{X}_l = \tilde{H}_l \otimes \mathbf{1}_n^\top$ ).

- **DNC2:** The class-means at the  $l$ -th layer form either an orthogonal basis or a simplex equiangular tight frame (ETF). As for DNC1, this property can be stated for features after or before  $\sigma$ . We write the ETF class-mean covariance  $\Sigma_{\text{ETF}} \triangleq (1 + \frac{1}{K-1})I_K - \frac{1}{K-1}\mathbf{1}_K\mathbf{1}_K^\top$ . In the former case, the condition requires either  $H_l^\top H_l \propto I_K$  or  $H_l^\top H_l \propto \Sigma_{\text{ETF}}$ ; in the latter  $\tilde{H}_l^\top \tilde{H}_l \propto I_K$  or  $\tilde{H}_l^\top \tilde{H}_l \propto \Sigma_{\text{ETF}}$ .

### 3.3 Average gradient outer product

The AGOP operator acts with respect to a dataset  $X \in \mathbb{R}^{d_0 \times N}$  and any model, that accepts inputs from the data domain  $f : \mathbb{R}^{d_0 \times 1} \rightarrow \mathbb{R}^{K \times 1}$ , where  $K$  is the number of outputs. Writing the Jacobian of the model outputs with respect to its inputs at layer  $l$  as  $\frac{\partial f(x)}{\partial x^l} \in \mathbb{R}^{d_0 \times K}$ , the AGOP is defined as:

$$\text{AGOP}(f, X) \triangleq \frac{1}{N} \sum_{c=1}^K \sum_{i=1}^N \frac{\partial f(x_{ci})}{\partial x} \frac{\partial f(x_{ci})^\top}{\partial x}.$$

This object has important implications for learning because the AGOP of a learned predictor will (with surprisingly few samples) resemble the *expected* gradient outer product (EGOP) of the target function [Yuan et al., 2023]. While the AGOP is specific to a model and training data, the EGOP is determined by the population data distribution and the function to be estimated, and contains specific useful information such as low-rank structure, that improves prediction.

Remarkably, it was identified in Radhakrishnan et al. [2024a], Beaglehole et al. [2023] that neural networks will automatically contain AGOP structure in the Gram matrix of the weights in all layers of the neural network, where the AGOP at each layer acts on the sub-network and feature vectors at that layer. Stated formally, the authors observe and pose the Neural Feature Ansatz (NFA):

**Ansatz 3.2** (Neural Feature Ansatz [Radhakrishnan et al., 2024a]). *Let  $f$  be a depth- $L$  neural network trained on data  $X$  using stochastic gradient descent. Then, for all layers  $l \in [L]$ ,*

$$\rho \left( W_l^\top W_l, \frac{1}{N} \sum_{c=1}^K \sum_{i=1}^n \frac{\partial f(x_{ci})}{\partial x^l} \frac{\partial f(x_{ci})^\top}{\partial x^l} \right) \approx 1.$$

The correlation function  $\rho$  accepts two matrix inputs of shapes  $(p_1, q_1)$  and  $(p_2, q_2)$  and returns their cosine similarity, whose value is in  $[-1, 1]$ .

Crucially, the AGOP can be defined for any differentiable estimator, not necessarily a neural network. In Radhakrishnan et al. [2024a], the authors introduce a kernel learning algorithm, the Recursive Feature Machine (RFM), that performs kernel regression and estimates the AGOP in an alternating fashion, modeling the NFA feature learning mechanism of fully-connected networks.

Subsequent work introduced the Deep Recursive Feature Machine (Deep RFM) to model deep feature learning in neural networks [Beaglehole et al., 2023]. Deep RFM iteratively generates representations by mapping the input to that layer with the AGOP of the model w.r.t. this input, and then applying an untrained random feature map. To define the Deep RFM, let  $\{k_l\}_{l=1}^{L+1} : \mathbb{R}^{d_l \times d_l} \rightarrow \mathbb{R}$  be a set of kernels. For the ease of notation, we will write  $k_l(X'_l, X_l)$  for a matrix of kernel evaluations between columns of  $X'_l$  and  $X_l$ . We then describe Deep RFM in Algorithm 1.

Note that the Deep RFM as defined here considers only one AGOP estimation step in the inner-optimization of RFM, while multiple iterations are used in Beaglehole et al. [2023]. The high-dimensional feature maps  $\Phi_l(\cdot)$  are usually realized as  $\sigma(W_l \cdot + b_l)$ , where  $W_l$  is a matrix with standard Gaussian entries,  $b_l$  is an optional bias term initialized uniformly at random, and  $\sigma$  is the ReLU or cosine activation function. Thus,  $\Phi_l$  typically serves as a random features generator.

The single loop in the Deep RFM represents a reduced RFM learning process. The RFM itself is based on kernel ridge regression, therefore we introduce the ridge coefficient  $\mu$ . The training procedure of RFM is meant to perform well in the corresponding kernel ridge regression which will be particularly important in Section 4.3.

## 4 Average gradient outer product induces DNC in Deep RFM

We demonstrate that AGOP is a mechanism for DNC in the Deep RFM model, which was proposed in prior work as an abstraction for deep feature learning in DNNs. We first demonstrate empirically

---

**Algorithm 1** Deep Recursive Feature Machine (Deep RFM)

---

**input**  $X_1, Y, \{k_l\}_{l=1}^{L+1}, L, \{\Phi_l\}_{l=1}^L$  {kernels:  $\{k_l\}_l$ , depth:  $L$ , feature maps:  $\{\Phi_l\}_l$ }  
**output**  $\alpha_{L+1}, \{M_l\}_{l=1}^L$   
**for**  $l \in 1, \dots, L$  **do**  
    Normalize the data,  $X_l \leftarrow X_l \oplus \|X_l\|$   
    Learn coefficients,  $\alpha_l = Y(k_l(X_l, X_l) + \mu I)^{-1}$ .  
    Construct predictor,  $f_l(\cdot) = \alpha_l k_l(\cdot, X_l)$ .  
    Compute AGOP:  $M_l = \sum_{c,i=1}^{K,n} \nabla f_l(x_{ci}^l) \nabla f_l(x_{ci}^l)^\top$ .  
    Transform the data  $X_{l+1} \leftarrow \Phi_l(M_l^{1/2} X_l)$ .  
**end for**  
Normalize the data,  $X_{L+1} \leftarrow X_{L+1} \oplus \|X_{L+1}\|$   
Learn coefficients,  
 $\alpha_{L+1} = Y(k_{L+1}(X_{L+1}, X_{L+1}) + \mu I)^{-1}$ .

---

that Deep RFM exhibits DNC - NC1 and NC2 - and that the induction of neural collapse is due to the application of AGOP. Finally, we prove theoretically in an asymptotic and non-asymptotic setting that DNC will occur as a consequence of Deep RFM.

#### 4.1 Empirical evidence

We visualize the formation of DNC in the input vectors of each layer of Deep RFM. Let  $\tilde{X}_l \equiv M_l^{1/2} X_l$  be the feature vectors at layer  $l$  projected onto the square root of the AGOP,  $M_l^{1/2}$ , at that layer, and let  $\tilde{\mu}^l$  be the average of the class means of  $\tilde{X}_l$ . In Figure 1, we show the Gram matrix,  $\tilde{X}_l \tilde{X}_l^\top$ , of centered and normalized feature vectors  $\bar{X}_l = (\tilde{X}_l - \tilde{\mu}^l) \oplus \|\tilde{X}_l - \tilde{\mu}^l\|$  extracted from several layers of Deep RFM, as presented in Algorithm 1, trained on CIFAR-10 and MNIST (see Appendix D for similar results on SVHN). After 18 layers of DeepRFM, the final Gram matrix is approximately equal to that of collapsed data, in which all points are at exactly their class means, and the centered class means form an ETF. Specifically, all centered points of the same class have inner product 1, while pairs of different class have inner product  $-(K-1)^{-1}$ .

We show collapse occurring as a consequence of projection onto the AGOP, across all datasets and across choices of feature map (Figures 3 and 4 in Appendix D). We observe that the improvement in NC1 is entirely due to  $M_l^{1/2}$ , and the random feature map actually worsens the NC1 value. This result is intuitive as Deep RFM deviates from a simple deep random feature model just by additionally projecting onto the AGOP with respect to the input at each layer, and we do not expect random feature maps to induce neural collapse on their own (shown formally in Appendix A).

#### 4.2 Asymptotic analysis

Many works have derived that, under mild conditions on the data and kernel, non-linear kernel matrices of high dimensional data are well approximated by linear kernels with a non-linear perturbation [Karoui, 2010, Adlam et al., 2019, Hu and Lu, 2022]. In this section, we provide a proof that Deep RFM will induce DNC when the non-linear kernels  $\{k_l\}_l$  and feature maps  $\{\Phi_l\}_l$  satisfy this property. In particular, in the high-dimensional setting in these works, non-linear kernel matrices written  $k(X) := k(X, X)$  for simplicity, are well approximated by

$$k(X) \approx \gamma_k \mathbf{1}\mathbf{1}^\top + X^\top X + \lambda_k I,$$

where  $\lambda_k, \gamma_k > 0$ . Following Adlam and Pennington [2020], for additional simplicity we consider centered kernels,  $k_{\text{lin}}(X) \equiv X^\top X + \lambda_k I$ .

We analyze the Deep RFM with two slight modifications: (i) we do not normalize the data at each iteration, and (ii) we scale the data by a value  $\kappa^{-1}$  at each iteration. The recursive procedure begins with a dataset  $X_l$  at layer  $l$  in Deep RFM, and constructs  $\tilde{X}_l$  from the AGOP  $M_l$  of the kernel

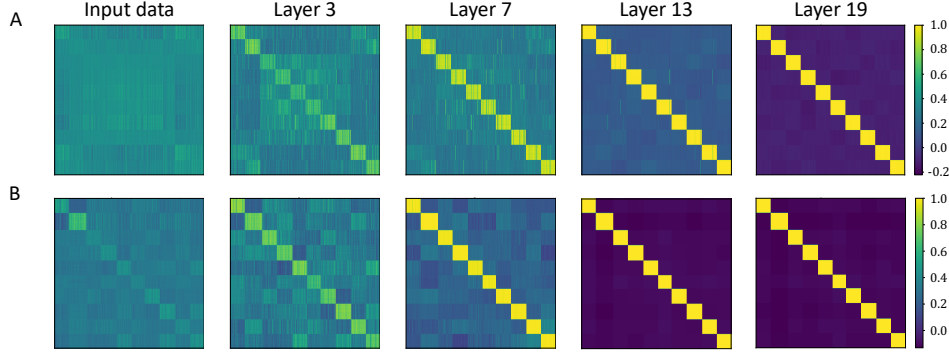


Figure 1: Neural collapse with Deep RFM on (A) CIFAR-10 and (B) MNIST. The matrix of inner products of all pairs of points in  $\tilde{X}_l$  extracted from layers  $l \in \{1, \dots, 19\}$  of Deep RFM, after applying  $M_l^{1/2}$ , centering by the global mean  $\mu_G^l$  and normalizing each data point. The data are ordered so that points of the same class are adjacent to one another, arranged from classes 1 to 10. Deep RFM uses non-linearity  $\sigma(\cdot) = \cos(\cdot)$  in (A) and  $\sigma(\cdot) = \text{ReLU}(\cdot)$  in (B).

ridgeless regression solution such that

$$\tilde{X}_{l+1}^\top \tilde{X}_{l+1} = \kappa^{-1} X_l^\top M_l X_l,$$

for  $\kappa = 1 - 2\lambda_k(1 + \lambda_\Phi^{-1})$ . Then, we will apply a non-linear feature map  $\Phi_{\text{lin}}$  corresponding to a kernel  $k_\Phi$  that exhibits a similar linearization on the data. For  $k_\Phi$ , we introduce a new parameter  $\lambda_\Phi$  capturing the deviation of this feature map from linearity, and write the corresponding Gram matrix

$$X_{l+1}^\top X_{l+1} = \Phi_{\text{lin}}(\tilde{X}_{l+1})^\top \Phi_{\text{lin}}(\tilde{X}_{l+1}) \equiv k_\Phi(\tilde{X}_{l+1}) = \tilde{X}_{l+1}^\top \tilde{X}_{l+1} + \lambda_\Phi I,$$

where  $\lambda_k, \lambda_\Phi$  are finite and  $\lambda_\Phi \gg \lambda_k > 0$ .

Intuitively, the ratio  $\lambda_k/\lambda_\Phi$  determines how close to linear  $k_{\text{lin}}$  is when applied to the dataset, and therefore the rate of NC. By Assumption 4.2, the scaled gram matrix  $\bar{G}_l \equiv \lambda_\Phi^{-1} X_l^\top X_l$  has minimum eigenvalue at least 1. Meanwhile, the scaled kernel matrix has the form

$$\lambda_\Phi^{-1} (X_l^\top X_l + \lambda_k I) = \bar{G}_l + \lambda_k/\lambda_\Phi \cdot I.$$

If  $\lambda_k/\lambda_\Phi$  were exactly 0, then  $(\bar{G}_l + \lambda_k/\lambda_\Phi \cdot I)^{-1}$  is equal to  $\bar{G}_l^{-1} = \lambda_\Phi (X_l^\top X_l)^{-1}$ , the scaled linear regression solution. In this case, collapse will occur in just one layer of Deep RFM, as the AGOP of a linear function is exactly the outer product of the solution with itself. Otherwise, if this ratio were large, i.e.  $\lambda_k/\lambda_\Phi = \Omega(1)$ ,  $(\bar{G}_l + \lambda_k/\lambda_\Phi \cdot I)^{-1}$  can be far from the linear regression solution. In this case, the kernel regression solution contains non-linear variations that increase the rank of the AGOP (preventing collapse). Between these limits, larger  $\lambda_k$  delays collapse across layers of Deep RFM, while larger  $\lambda_\Phi$  accelerates collapse. Note that this theory offers an explanation why a non-linear activation is needed for DNC:  $\lambda_\Phi = 0$  with a linear feature map.

We provide a simple interpretation for why non-linear feature maps introduce an identity term  $\lambda_\Phi I$  to the data Gram matrix. As in our experiments on Deep RFM where  $\Phi(x) = \sigma(Wx)$ , the random feature map separates all pairs of data points, especially nearby ones, lowering the off-diagonal entries in the empirical kernel and increasing the effective rank of this matrix (see Appendix A for a formal derivation of this fact).

We prove that DNC occurs in the following full-rank, high-dimensional setting.

**Assumption 4.1** (Data is high dimensional). We assume that the data has dimension  $d \geq n$ .

**Assumption 4.2** (Data is full rank). We assume that the initial data Gram matrix  $X_1^\top X_1$  has minimum eigenvalue at least  $\lambda_\phi > 0$ . Otherwise the theorem holds for  $l > 2$ , after the feature map is applied.

Our particular analysis requires these assumptions to guarantee  $(X_l^\top X_l)^{-1}$  is stable (i.e. it exists and has maximum eigenvalue  $\lambda_\Phi^{-1}$  at every iteration) for all  $l$  in order to simplify the kernel ridge regression solution (see the proof in Appendix B).

We present our main theorem.

**Theorem 4.3** (Deep RFM exhibits neural collapse). *Suppose we apply Deep RFM on any dataset with  $\{\Phi_l\}_l$  and  $\{k_l\}_l$  all chosen as the feature map  $\Phi_{\text{lin}}$  and kernel  $k_{\text{lin}}$  above, with no ridge parameter ( $\mu = 0$ ). Then, there exists a universal constant  $C > 0$ , such that for any  $0 < \epsilon \leq 1$ , provided  $\lambda_k \leq \frac{C\lambda_\Phi}{2(1+\lambda_\Phi^{-1})^n}(1 - \epsilon)$ , and for all layers  $l \in \{2, \dots, L\}$  of Deep RFM,*

$$\|\tilde{X}_{l+1}^\top \tilde{X}_{l+1} - yy^\top\| \leq (1 - \epsilon)\|\tilde{X}_l^\top \tilde{X}_l - yy^\top\| + O(\lambda_k^2 \lambda_\Phi^{-2}).$$

Note that this theorem immediately implies exponential convergence to NC1 and NC2 up to error  $O(L\lambda_k^2 \lambda_\Phi^{-2})$ , a small value determined by the parameters of the problem. As a validation of our theory, we see that this exponential improvement in the DNC metric occurs in all layers (see Figures 3 and 4). Note the exponential rate predicted by Theorem 4.3 and observed empirically for Deep RFM is consistent with the exponential rate observed in deep neural networks [He and Su, 2022].

The proof for this theorem is roughly as follows. Recall that, by our argument earlier in this section, a linear kernel will cause collapse within just one layer of Deep RFM. However, in the more general case we consider, a small non-linear deviation from a linear kernel,  $\lambda_k$ , is introduced. Beginning with the first layer, partial collapse occurs if the ratio  $\lambda_k \lambda_\Phi^{-1}$  is sufficiently small. Following the partial collapse, in subsequent layers, the data Gram matrix will sufficiently resemble the collapsed matrix, so that the non-linear kernel solution on the collapsed data will behave like the linear solution, leading to further convergence to the collapsed data Gram matrix, a fixed point of the Deep RFM iteration (Lemma B.2).

### 4.3 Non-asymptotic analysis

Next, we show that the formation of the neural collapse is not only implicitly given by the specific optimization procedure of the Deep RFM, but is also implicitly regularized for in the parametrized kernel ridge regression, a model class that includes RFM (i.e., a single layer of Deep RFM). Since we are in the multi-class classification setting, we need to consider vector-valued reproducing kernel Hilbert spaces (RKHS) and matrix-valued kernels.

Consider a separable matrix-valued kernel  $k_M : \mathcal{R}^d \times \mathcal{R}^d \rightarrow \mathcal{R}^C \times \mathcal{R}^C$  such that the input-level kernel is of the form  $\tilde{k}_M(x, y) = \phi(\|x - y\|_M^2)$ , where  $\|x - y\|_M^2 = (x - y)^\top M(x - y)$ ,  $\phi$  is a strictly decreasing, strictly positive univariate function s.t.  $\phi(0) = 1$ , and  $k_M$  is a valid kernel for any symmetric positive semi-definite  $M$ . The output-dimension level kernel\* is fixed to be the identity. Let  $\mathcal{H}_M$  be the corresponding vector-valued RKHS. Then, by the parametrized kernel ridge regression, we mean the following optimization problem over all possible  $M$  and  $f \in \mathcal{H}_M$ :

$$\min_{f, M} \frac{1}{2} \|f(X) - Y\|^2 + \frac{\mu}{2} \|f\|_{\mathcal{H}_M}^2. \quad (1)$$

An analog of the representer theorem for vector-valued RKHS can be shown [Ciliberto et al., 2015, Micchelli and Pontil, 2004] and therefore the optimal solution of (1) can be written as  $f(z) = \sum_{c, i=1,1}^{K, n} \alpha_{ci} k_M(x_{ci}, z)$ , where  $\alpha_{ci}$  is a  $K$ -dimensional vector. Let us therefore denote  $A$  the matrix of stacked columns  $\alpha_{ci}$ . We can re-formulate Problem 1 as the following finite-dimensional optimization problem:

$$\min_{A, M} \text{tr}((Y - Ak_M)(Y - Ak_M)^T) + \lambda \text{tr}(k_M A^T A), \quad (2)$$

where  $k_M := k_M(X, X)$  is the matrix of pair-wise kernel evaluations on the data. This computation is not trivial, but closely follows standard practices in multi-task kernel ridge regression. Since we do not explicitly regularize  $M$ , we will drop the dependence on it, treat  $k$  as a free optimization variable and compute the optimal value of the following relaxed problem:  $\min_{A, k} \text{tr}((Y - Ak)(Y - Ak)^T) + \lambda \text{tr}(k A^T A)$ . This can be equivalently written as:

$$\min_{A, k} \text{tr}(A(k^2 + \mu k)A^T) - 2 \text{tr}(AkY^T). \quad (3)$$

We are now ready to state our optimality theorem.

\*Also called task-level kernel from the multi-task learning context, where vector-valued RKHS is most often used in machine learning.

**Theorem 4.4.** *The optimal limiting solution of the Problem 3 is  $k^* = I_C \otimes (\mathbf{1}_n \mathbf{1}_n^\top) = yy^\top$ . Any positive definite  $k$  sufficiently close to this (positive semi-definite) solution is therefore nearly optimal.*

We provide a sketch here and defer a detailed proof to Appendix B.

*Proof.* Let  $\mathcal{L}(A, k) = \text{tr}(A(k^2 + \mu k)A^\top) - 2 \text{tr}(AkY^\top)$ . Due to the separability of Problem 2 in the rows of  $A$ , we can solve for  $A$  assuming fixed  $k$  and thus reduce the Problem 2 to:  $\max_k \sum_{c=1}^C y_c^\top (k + \mu I)^{-1} k y_c$ . From the eigenvalue decomposition of  $K \equiv VSV^\top$ , this is equivalent to:

$$\max_k \sum_{c=1}^C \sum_{i=1}^{Cn} (y_c^\top v_i)^2 \frac{\lambda_i}{\lambda_i + \mu}, \quad (4)$$

where  $\lambda_i, v_i$  are the  $i$ -th eigenvalue and eigenvector, respectively. Using continuity arguments, we have that  $\mathcal{L}(A^*, k^*) = Cn \frac{n}{n+\mu}$ . With slight abuse of notation, let us now re-scale  $Y$  so that each row is unit-norm and divide the loss  $\mathcal{L}$  by  $C$ . Then we get (abusing the notation):  $\mathcal{L}(A^*, k^*) = \frac{n}{n+\mu}$ . Now,  $\sum_{i=1}^{Cn} (y_c^\top v_i)^2 = 1$  since  $(v_i)_{i=1}^{Cn}$  forms an orthogonal basis and, thus, a tight frame with constant 1. Therefore, the expression in (4) can be viewed as a weighted average of the  $\frac{\lambda_i}{\lambda_i + \mu}$  terms. To simplify the expression, denote  $\omega_i := \frac{1}{C} \sum_{c=1}^C (y_c^\top v_i)^2$ . Using Cauchy-Schwarz inequality on each individual summand, we see that  $(y_c^\top v_i)^2 \leq \sum_{j; y_{cj}=1} v_{ij}^2$  and the equality is only achieved if all the entries of  $v_i$  corresponding to entries of  $y_c$  equal to 1 are the same. Thus,  $\sum_{c=1}^C (y_c^\top v_i)^2 \leq \|v_i\|^2 = 1$  with equality if and only if, for each  $c$ , all the entries of  $v_i$  corresponding to the entries of  $y_c$  equal to 1 are the same. This gives that  $\omega_i \leq \frac{1}{C}$ .

For any feasible  $k$ , we have  $\mathcal{L}(k, \alpha^*) = \sum_{i=1}^{Cn} \omega_i \frac{\lambda_i}{\lambda_i + \mu} \leq \frac{1}{C} \sum_{i=1}^C \frac{\lambda_i}{\lambda_i + \mu} < \frac{\frac{1}{C} \sum_{i=1}^C \lambda_i}{\frac{1}{C} \sum_{i=1}^C \lambda_i + \mu} \leq \frac{n}{n+\mu}$ . The first inequality is due to the monotonicity of  $g(x) = \frac{x}{x+\mu}$  and  $\omega_i \leq \frac{1}{C}$ ; the second strict inequality is due to Jensen after noting that  $g$  is strictly convex and using the Perron-Frobenius theorem which says that  $\lambda_1$  has multiplicity 1; and the last inequality is due to  $\sum_{i=1}^{Cn} \lambda_i = Cn$ , which follows from the fact that  $k$  must have all the diagonal elements equal to 1. This concludes the proof.  $\square$

## 5 DNC as an effect of linear denoising in neural networks

We link the DNC mechanism of Deep RFM, i.e., the projection onto the AGOP, to DNC formation in typical neural networks, such as MLPs, VGG, and ResNet. We do so by providing evidence that DNC occurs by this iterated linear mechanism through the right singular structure of the weights.

There are precisely two ways in which DNNs can discard unnecessary information in the data, such as noise or spurious features. One of them is through non-linearities, i.e., ReLU, where negative entries are erased. The other one is through the small eigendirections of  $W_l^\top W_l$  or, approximately, the non-trivial null space of  $W_l$ , where components of vectors that belong to the null space are discarded. If we write again the SVD  $W_l = U_l S_l V_l^\top$ , then  $S_l V_l^\top$  is the part with possibly non-trivial null space. This right singular component can be viewed as the *feature extraction* part of the linear layer. In contrast, the multiplication with  $U_l$  simply rotates or reflects the prior representation.

All parts of the process, together with the non-linearity, are important for inference via the neural network. However, the DNC1 can only improve through the  $S_l V_l^\top$  multiplication and the application of the non-linearity. In particular, considering the standard DNC1 metric  $\text{tr}(\Sigma_W) \text{tr}(\Sigma_B)^{-1}$  [Tirer et al., 2023, Rangamani et al., 2023], a simple computation using the cyclic property of the trace gives  $\text{tr}(\hat{\Sigma}_W) \text{tr}(\hat{\Sigma}_B)^{-1} = \text{tr}(U \Sigma_W U^\top) \text{tr}(U \Sigma_B U^\top)^{-1} = \text{tr}(\Sigma_W) \text{tr}(\Sigma_B)^{-1}$ . The  $\Sigma$  matrices refer to the within-class variability after the application of  $SV^\top$ , while the  $\hat{\Sigma}$  matrices correspond to the output of the full weight matrix.

While both non-linearity and  $S_l V_l^\top$  can influence the DNC1 metric, we demonstrate that, in a variety of settings,  $S_l V_l^\top$  is responsible for directly inducing the majority of within-class variability collapse. We verify this claim by plotting the DNC1 metrics of all layers of an MLP and ResNet network trained on MNIST and CIFAR-10, respectively (Figure 2), where each layer is decomposed into its different parts – (1) the input to that layer, (2) the embedding after multiplication with  $S_l V_l^\top$ , and (3) the embedding after multiplication with the left singular vectors and application of the non-linearity.



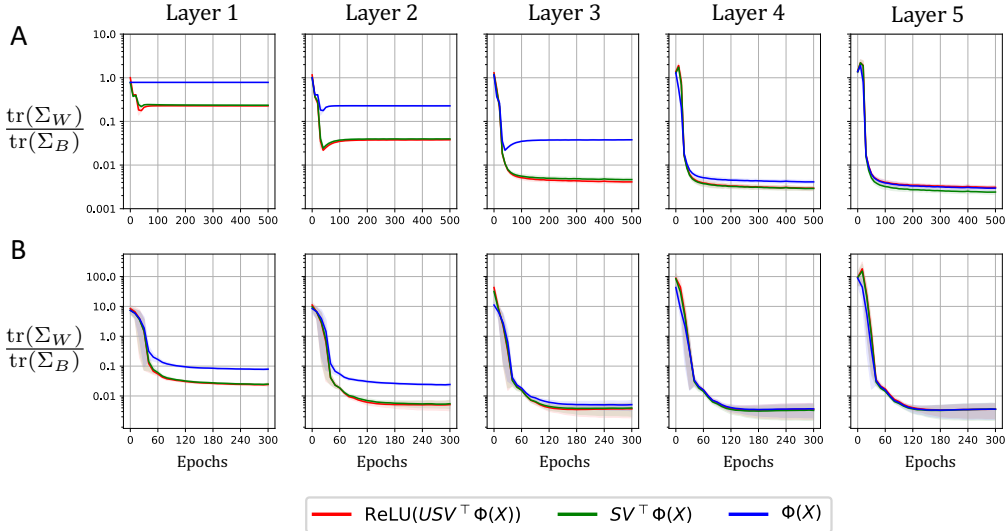


Figure 2: Feature variability collapse from different singular value decomposition components in (A) an MLP on MNIST, and (B) a ResNet on CIFAR-10. We measure the reduction in the NC1 metric throughout training at each of five fully-connected layers. Each layer is decomposed into its input,  $\Phi(X)$ , the projection onto the right singular space of  $W$ ,  $SV^T \Phi(X)$ , and then  $U$ , the left singular vectors of  $W$ , and the application of the non-linearity.

We see that the ratio of within-class to between-class variability decreases mostly between steps (1) and (2), due to the application of the right singular structure. This has profound implications for neural collapse, as it shows that DNNs can cancel most of the intra-class sample differences (which, assuming neural collapse preserves task-relevant information, is the irrelevant variation in the data) by the linear weight matrix, and not the non-linearity. Similar results are in Appendix D for all combinations of datasets (MNIST, CIFAR-10, SVHN) and architectures (MLP, VGG, and ResNet).

We note that, while in this setting the ReLU does not directly reduce NC1, the ReLU is still crucial for ensuring the expressivity of the feature vectors. Without non-linearity, the neural network cannot interpolate the data or perform proper feature learning, necessary conditions for DNC to occur at all.

These results are in a regime where the NFA holds with high correlation, with ResNet and MLP having NFA correlations at the end of training (averaged over all layers and seeds) of  $0.74 \pm 0.17$  and  $0.74 \pm 0.13$  on CIFAR-10 and MNIST, respectively (see Appendix D for values across all architectures and datasets). Thus,  $S_l V_l^T$  should project into a similar space as the AGOP. We note that the matrix quantities involved are high-dimensional, and the trivial correlation between two i.i.d. uniform eigenvectors of dimension  $d$  concentrates within  $\pm O(d^{-1/2})$ . For the width 512 weight matrices considered here, this correlation would be approximately (at most) 0.04. Therefore, we conclude that the AGOP structure can decrease within-class variability in DNNs.

Unlike DNC1, we have observed a strong DNC2 progression only in the very last layer. This is due to the fact that DNC2 was observed in the related work Rangamani et al. [2023], Parker et al. [2023] in a regime of large initialization. In contrast, the NFA holds most consistently with small initialization [Radhakrishnan et al., 2024a], and in this feature learning regime, the low-rank bias prevents strong collapse from occurring, see Li et al. [2020] for a good intuition on this low-rank bias.

## 6 Conclusion

This work establishes that deep neural collapse can occur through feature learning with the AGOP. We bridge the unsatisfactory gap between DNC and the data – with previous work mostly only focusing on the very end of the network and ignoring the training data.

First, we demonstrate that projection onto the AGOP induces deep neural collapse in Deep RFM. We validate that AGOP induces NC in Deep RFM both empirically and via asymptotic and non-asymptotic theoretical analyses.

Second, we experimentally show that the DNC1 metric progression through the layers can be mostly due to the linear denoising via the application of the center-right singular structure. Through the neural feature ansatz, the application of this structure is approximately equivalent to projection onto the AGOP, suggesting that AGOP can induce neural collapse also in typical DNNs.

## Acknowledgements

We acknowledge support from the National Science Foundation (NSF) and the Simons Foundation for the Collaboration on the Theoretical Foundations of Deep Learning through awards DMS-2031883 and #814639 as well as the TILOS institute (NSF CCF-2112665). This work used the programs (1) XSEDE (Extreme science and engineering discovery environment) which is supported by NSF grant numbers ACI-1548562, and (2) ACCESS (Advanced cyberinfrastructure coordination ecosystem: services & support) which is supported by NSF grants numbers #2138259, #2138286, #2138307, #2137603, and #2138296. Specifically, we used the resources from SDSC Expanse GPU compute nodes, and NCSA Delta system, via allocations TG-CIS220009. Marco Mondelli is supported by the 2019 Lopez-Loreta prize.

## References

- Ben Adlam and Jeffrey Pennington. The neural tangent kernel in high dimensions: Triple descent and a multi-scale theory of generalization. In *International Conference on Machine Learning*, pages 74–84. PMLR, 2020.
- Ben Adlam, Jake Levinson, and Jeffrey Pennington. A random matrix perspective on mixtures of nonlinearities for deep learning. *arXiv preprint arXiv:1912.00827*, 2019.
- Daniel Beaglehole, Adityanarayanan Radhakrishnan, Parthe Pandit, and Mikhail Belkin. Mechanism of feature learning in convolutional neural networks. *arXiv preprint arXiv:2309.00570*, 2023.
- Daniel Beaglehole, Ioannis Mitliagkas, and Atish Agarwala. Gradient descent induces alignment between weights and the empirical ntk for deep non-linear networks. *arXiv preprint arXiv:2402.05271*, 2024.
- Carlo Ciliberto, Youssef Mroueh, Tomaso Poggio, and Lorenzo Rosasco. Convex learning of multiple tasks and their structure. In *International Conference on Machine Learning*, pages 1548–1557. PMLR, 2015.
- Cong Fang, Hangfeng He, Qi Long, and Weijie J Su. Exploring deep neural networks via layer-peeled model: Minority collapse in imbalanced training. In *Proceedings of the National Academy of Sciences (PNAS)*, volume 118, 2021.
- Tomer Galanti, András György, and Marcus Hutter. Improved generalization bounds for transfer learning via neural collapse. In *First Workshop on Pre-training: Perspectives, Pitfalls, and Paths Forward at ICML*, 2022.
- Jarrod Haas, William Yolland, and Bernhard T Rabus. Linking neural collapse and l2 normalization with improved out-of-distribution detection in deep neural networks. *Transactions on Machine Learning Research (TMLR)*, 2022.
- X. Y. Han, Vardan Papyan, and David L Donoho. Neural collapse under mse loss: Proximity to and dynamics on the central path. In *International Conference on Learning Representations (ICLR)*, 2022.
- Hangfeng He and Weijie J Su. A law of data separation in deep learning. *arXiv preprint arXiv:2210.17020*, 2022.
- Wanli Hong and Shuyang Ling. Neural collapse for unconstrained feature model under cross-entropy loss with imbalanced data. *arXiv preprint arXiv:2309.09725*, 2023.

- Hong Hu and Yue M Lu. Universality laws for high-dimensional learning with random features. *IEEE Transactions on Information Theory*, 69(3):1932–1964, 2022.
- Wenlong Ji, Yiping Lu, Yiliang Zhang, Zhun Deng, and Weijie J Su. An unconstrained layer-peeled perspective on neural collapse. In *International Conference on Learning Representations (ICLR)*, 2022.
- Noureddine El Karoui. The spectrum of kernel random matrices. *The Annals of Statistics*, pages 1–50, 2010.
- Vignesh Kothapalli. Neural collapse: A review on modelling principles and generalization. In *Transactions on Machine Learning Research (TMLR)*, 2023.
- Daniel Kunin, Atsushi Yamamura, Chao Ma, and Surya Ganguli. The asymmetric maximum margin bias of quasi-homogeneous neural networks. *arXiv preprint arXiv:2210.03820*, 2022.
- Zhiyuan Li, Yuping Luo, and Kaifeng Lyu. Towards resolving the implicit bias of gradient descent for matrix factorization: Greedy low-rank learning. *arXiv preprint arXiv:2012.09839*, 2020.
- Jianfeng Lu and Stefan Steinerberger. Neural collapse under cross-entropy loss. In *Applied and Computational Harmonic Analysis*, volume 59, 2022.
- Charles Micchelli and Massimiliano Pontil. Kernels for multi-task learning. *Advances in neural information processing systems*, 17, 2004.
- Dustin G Mixon, Hans Parshall, and Jianzong Pi. Neural collapse with unconstrained features. *arXiv preprint arXiv:2011.11619*, 2020.
- Vardan Papyan, X. Y. Han, and David L Donoho. Prevalence of neural collapse during the terminal phase of deep learning training. In *Proceedings of the National Academy of Sciences (PNAS)*, volume 117, 2020.
- Liam Parker, Emre Onal, Anton Stengel, and Jake Intrater. Neural collapse in the intermediate hidden layers of classification neural networks. *arXiv preprint arXiv:2308.02760*, 2023.
- Tomaso Poggio and Qianli Liao. Explicit regularization and implicit bias in deep network classifiers trained with the square loss. *arXiv preprint arXiv:2101.00072*, 2020.
- Adityanarayanan Radhakrishnan, Daniel Beaglehole, Parthe Pandit, and Mikhail Belkin. Mechanism for feature learning in neural networks and backpropagation-free machine learning models. *Science*, 383(6690):1461–1467, 2024a.
- Adityanarayanan Radhakrishnan, Mikhail Belkin, and Dmitriy Drusvyatskiy. Linear recursive feature machines provably recover low-rank matrices. *arXiv preprint arXiv:2401.04553*, 2024b.
- Akshay Rangamani, Marius Lindgaard, Tomer Galanti, and Tomaso Poggio. Feature learning in deep classifiers through intermediate neural collapse. *Technical Report*, 2023.
- Jingtong Su, Ya Shi Zhang, Nikolaos Tsilivis, and Julia Kempe. On the robustness of neural collapse and the neural collapse of robustness. *arXiv preprint arXiv:2311.07444*, 2023.
- Peter Sůkeník, Marco Mondelli, and Christoph Lampert. Deep neural collapse is provably optimal for the deep unconstrained features model. *arXiv preprint arXiv:2305.13165*, 2023.
- Christos Thrampoulidis, Ganesh Ramachandra Kini, Vala Vakilian, and Tina Behnia. Imbalance trouble: Revisiting neural-collapse geometry. In *Conference on Neural Information Processing Systems (NeurIPS)*, 2022.
- Tom Tirer and Joan Bruna. Extended unconstrained features model for exploring deep neural collapse. In *International Conference on Machine Learning (ICML)*, 2022.
- Tom Tirer, Haoxiang Huang, and Jonathan Niles-Weed. Perturbation analysis of neural collapse. *arXiv preprint arXiv:2210.16658*, 2022.

- Tom Tirer, Haoxiang Huang, and Jonathan Niles-Weed. Perturbation analysis of neural collapse. In *International Conference on Machine Learning*, pages 34301–34329. PMLR, 2023.
- Peng Wang, Huikang Liu, Can Yaras, Laura Balzano, and Qing Qu. Linear convergence analysis of neural collapse with unconstrained features. In *OPT 2022: Optimization for Machine Learning (NeurIPS 2022 Workshop)*, 2022.
- Zijian Wang, Yadan Luo, Liang Zheng, Zi Huang, and Mahsa Baktashmotlagh. How far pre-trained models are from neural collapse on the target dataset informs their transferability. In *Proceedings of the IEEE/CVF International Conference on Computer Vision*, pages 5549–5558, 2023.
- E Weinan and Stephan Wojtowytsch. On the emergence of simplex symmetry in the final and penultimate layers of neural network classifiers. In *Mathematical and Scientific Machine Learning*, 2022.
- Max A Woodbury. *Inverting modified matrices*. Department of Statistics, Princeton University, 1950.
- Mengjia Xu, Akshay Rangamani, Qianli Liao, Tomer Galanti, and Tomaso Poggio. Dynamics in deep classifiers trained with the square loss: Normalization, low rank, neural collapse, and generalization bounds. In *Research*, volume 6, 2023.
- Gan Yuan, Mingyue Xu, Samory Kpotufe, and Daniel Hsu. Efficient estimation of the central mean subspace via smoothed gradient outer products. *arXiv preprint arXiv:2312.15469*, 2023.
- Jinxin Zhou, Xiao Li, Tianyu Ding, Chong You, Qing Qu, and Zhihui Zhu. On the optimization landscape of neural collapse under mse loss: Global optimality with unconstrained features. In *International Conference on Machine Learning (ICML)*, 2022.
- Libin Zhu, Chaoyue Liu, Adityanarayanan Radhakrishnan, and Mikhail Belkin. Catapults in sgd: spikes in the training loss and their impact on generalization through feature learning. *arXiv preprint arXiv:2306.04815*, 2023.

## A Random features cannot significantly reduce within-class variability

In the following proposition, we prove that the random features mapping with ReLU influences the within- and between-class variabilities only marginally and if anything, it makes the DNC1 metrics slightly worse.

**Proposition A.1.** *Let  $x, y \in \mathbb{R}^d$  be two fixed vectors of unit length. Let  $W \in \mathbb{R}^{D \times d}$  be a weight matrix whose entries are initialized i.i.d. from  $\mathcal{N}(0, 2/D)$ . Assume  $x^\top y = r$ . Then, for  $\sigma(\cdot) = \text{ReLU}(\cdot)$ ,*

$$\begin{aligned} \mathbb{E}(\sigma(Wx)^\top \sigma(Wy)) &= \frac{(1-r^2)^{3/2}}{\pi} + \frac{r^2 \sqrt{1-r^2}}{\pi} \\ &\quad + \frac{r}{2} + \frac{r}{\pi} \arctan\left(\frac{r}{\sqrt{1-r^2}}\right). \end{aligned} \quad (5)$$

*Moreover, the variance of this dot product scales with  $1/D$ , and the product is sub-exponential, making it well-concentrated.*

The proof is a direct computation, which is deferred to Appendix B.

This proposition gives a relationship between the dot product  $x^\top y$  of two vectors and the dot product of the outputs of their corresponding random feature maps  $\sigma(Wx)^\top \sigma(Wy)$ . This is relevant because for unit vectors, the dot product is a direct indication of the distance between the two vectors.

This means that the distances between data points generally increase, but not drastically. They increase irrespective of the angle between data points, however they tend to expand relatively more, if the data points are already aligned. Therefore, the DNC1 metric should on average marginally increase or stay constant. This is in agreement with our Deep RFM measurements on all vision datasets (Appendix D). Importantly, this also supports the connection between neural networks and Deep RFM, since in DNNs the DNC1 metric also may not significantly change after applying the ReLU (Figure 2).

## B Proofs

### B.1 Asymptotic results

**Lemma B.1** (Woodbury Inverse Formula [Woodbury, 1950]).

$$(P + UV^\top)^{-1} = P^{-1} - P^{-1}U(I + V^\top P^{-1}U)^{-1}V^\top P^{-1}.$$

**Lemma B.2** (Fixed point of collapse). *Let  $A^* = yy^\top + \lambda_\Phi I$ , the collapsed data gram matrix following an application of the non-linear random feature map  $\Phi$ . Then,*

$$(A^*)^{-1} = \lambda_\Phi^{-1}I - \lambda_\Phi^{-1}(\lambda_\Phi + n)^{-1}yy^\top.$$

*Proof of Lemma B.2.* We write  $yy^\top = nUU^\top$ , where  $U \in \mathbb{R}^{n \times K}$  is the matrix of normalized eigenvectors of  $yy^\top$ . By Lemma B.1 and that  $U^\top U = I$ ,

$$\begin{aligned} (A^*)^{-1} &= (\lambda_\Phi I + nUU^\top)^{-1} \\ &= \lambda_\Phi^{-1}I - \frac{n}{\lambda_\Phi^2}U(I + n\lambda_\Phi^{-1}U^\top U)^{-1}U^\top \\ &= \lambda_\Phi^{-1}I - \frac{n}{\lambda_\Phi^2} \cdot \frac{1}{1 + n\lambda_\Phi^{-1}}UU^\top \\ &= \lambda_\Phi^{-1}I - \frac{n}{\lambda_\Phi(\lambda_\Phi + n)}UU^\top \\ &= \lambda_\Phi^{-1}I - \frac{\lambda_\Phi^{-1}}{\lambda_\Phi + n}yy^\top. \end{aligned}$$

□

*Proof of Proposition 4.3.* We have solved the kernel ridgeless regression problem to get coefficients  $\alpha = (X_l X_l^\top + \lambda_k I)^{-1} y$ . Then, the predictor at layer  $l$  evaluated on the training data is,

$$f_l(X_l) = (X_l^\top X_l + \lambda_k I) \alpha .$$

As in Deep RFM, let  $M$  be the AGOP. Then,

$$M = \sum_{i=1}^n \nabla f(x^{(i)}) (\nabla f(x^{(i)}))^\top = X_l \alpha \alpha^\top X_l^\top .$$

We drop the subscript  $l$  for simplicity. Therefore,

$$X^\top M X = X^\top X (X^\top X + \lambda_k I)^{-1} y y^\top (X^\top X + \lambda_k I)^{-1} X^\top X .$$

Let  $A = X^\top X$ . Applying Lemma B.1,

$$(A + \lambda_k I)^{-1} = A^{-1} - \lambda_k A^{-1} (I + \lambda_k A^{-1})^{-1} A^{-1} .$$

Therefore,

$$X^\top M X = \left( I - \lambda_k (I + \lambda_k A^{-1})^{-1} A^{-1} \right) y y^\top \left( I - \lambda_k (I + \lambda_k A^{-1})^{-1} A^{-1} \right) .$$

Applying that, by assumption,  $\lambda_k \lambda_\Phi^{-1}$  is a small value  $\epsilon_{\text{lin}}$ , and as  $\lambda_\Phi$  is the minimum eigenvalue of  $A$ , we have that  $\lambda_k \|A^{-1}\| \leq \lambda_k \lambda_\Phi^{-1} \triangleq \epsilon_{\text{lin}}$ . Therefore,  $(I + \lambda_k A^{-1})^{-1} \lambda_k A^{-1} = \lambda_k A^{-1} - (\lambda_k A^{-1})^2 + \dots = \lambda_k A^{-1} + O(\epsilon_{\text{lin}}^2)$ , where  $O(\epsilon_{\text{lin}}^2)$  refers to some matrix of spectral norm at most  $C \epsilon_{\text{lin}}^2$  for some constant  $C > 0$ . Then,

$$X^\top M X = (I - \lambda_k A^{-1} + O(\epsilon_{\text{lin}}^2)) y y^\top (I - \lambda_k A^{-1} + O(\epsilon_{\text{lin}}^2)) = y y^\top - \lambda_k A^{-1} y y^\top - \lambda_k y y^\top A^{-1} + O(\epsilon_{\text{lin}}^2) .$$

Let  $\tilde{A} = \frac{A - A^*}{\|A - A^*\|}$ , and  $\epsilon_A = \|A - A^*\|$ . Then, applying Lemma B.1,

$$A^{-1} = \left( A^* + \epsilon_A \tilde{A} \right)^{-1} = \left( I + \epsilon_A (A^*)^{-1} \tilde{A} \right)^{-1} (A^*)^{-1} = (A^*)^{-1} - \epsilon_A (A^*)^{-1} \left( I + \epsilon_A \tilde{A} (A^*)^{-1} \right)^{-1} \tilde{A} (A^*)^{-1} .$$

Let  $\tilde{\Psi} = \left( I + \epsilon_A \tilde{A} (A^*)^{-1} \right)^{-1}$ . Assuming partial collapse has already occurred, i.e.,  $\epsilon_A \lambda_\Phi^{-1} < 1/2$ ,

$$\|\tilde{\Psi}\| \leq (1 - \epsilon_A \lambda_\Phi^{-1})^{-1} \leq 2 .$$

In this case, using that  $y y^\top (A^*)^{-1} = (A^*)^{-1} y y^\top = (1 + \lambda_\Phi^{-1}) y y^\top$  (Lemma B.2),

$$\begin{aligned} X^\top M X &= y y^\top - \lambda_k A^{-1} y y^\top - \lambda_k y y^\top A^{-1} + O(\epsilon_{\text{lin}}^2) \\ &= y y^\top - \lambda_k (A^*)^{-1} y y^\top - \lambda_k y y^\top (A^*)^{-1} + O(\epsilon_{\text{lin}}^2) \\ &\quad - \lambda_k \epsilon_A (A^*)^{-1} \tilde{\Psi} \tilde{A} (A^*)^{-1} y y^\top - \lambda_k \epsilon_A y y^\top (A^*)^{-1} \tilde{A} \tilde{\Psi} (A^*)^{-1} \\ &= y y^\top - 2\lambda_k (1 + \lambda_\Phi^{-1}) y y^\top + O(\epsilon_{\text{lin}}^2) \\ &\quad - \lambda_k \epsilon_A (1 + \lambda_\Phi^{-1}) (A^*)^{-1} \tilde{\Psi} \tilde{A} y y^\top - \lambda_k \epsilon_A (1 + \lambda_\Phi^{-1}) y y^\top \tilde{A} \tilde{\Psi} (A^*)^{-1} . \end{aligned}$$

Therefore, where  $\kappa = 1 - 2\lambda_k (1 + \lambda_\Phi^{-1}) > 1/2$  by choice of  $\lambda_k \cdot 2\lambda_\Phi^{-1} (1 + \lambda_\Phi^{-1}) n < 1 - \epsilon$ ,

$$\begin{aligned} \|X_{l+1}^\top X_{l+1} - A^*\| &= \|\kappa^{-1} X^\top M X - y y^\top\| \\ &= \left\| O(\epsilon_{\text{lin}}^2) + \epsilon_A \cdot \lambda_k \cdot 2\kappa^{-1} (1 + \lambda_\Phi^{-1}) (A^*)^{-1} \tilde{\Psi} \tilde{A} y y^\top \right\| \\ &\leq O(\epsilon_{\text{lin}}^2) + \epsilon_A \cdot \lambda_k \cdot 2\lambda_\Phi^{-1} (1 + \lambda_\Phi^{-1}) n \\ &< O(\epsilon_{\text{lin}}^2) + \epsilon_A (1 - \epsilon) \\ &= O(\epsilon_{\text{lin}}^2) + (1 - \epsilon) \|X_l X_l^\top - A^*\| . \end{aligned}$$

It remains to show that partial collapse,  $\epsilon_A \lambda_\Phi^{-1} < 1/2$ , happens in the first iteration. To ensure this condition, recall,

$$X^\top M X = y y^\top - \lambda_k A^{-1} y y^\top - \lambda_k y y^\top A^{-1} + O(\epsilon_{\text{lin}}^2) .$$

Therefore, because  $\|A^{-1}\| \leq \lambda_\Phi^{-1}$ , where  $\Psi$  is some error matrix with norm 1,

$$X^\top M X = y y^\top + \lambda_k \lambda_\Phi^{-1} n \Psi + O(\lambda_k^2 \lambda_\Phi^{-2}) .$$

Therefore,

$$\|X^\top M X - y y^\top\| < 1/2 ,$$

provided  $\lambda_k \lambda_\Phi^{-1} n < C_1/2$ , for some universal constant  $C_1$ .  $\square$

## B.2 Non-asymptotic results

**Theorem 4.4.** *The optimal limiting solution of the Problem 3 is  $k^* = I_C \otimes (\mathbf{1}_n \mathbf{1}_n^\top) = yy^\top$ . Any positive definite  $k$  sufficiently close to this (positive semi-definite) solution is therefore nearly optimal.*

*Proof.* Denote  $\mathcal{L}(A, k) = \text{tr}(A(k^2 + \mu k)A^\top) - 2 \text{tr}(AkY^\top)$ . Note that this problem is separable in the rows of  $A$ . If we only look at one row of  $A$  at a time, we can solve this problem explicitly for that row if we assume that  $k$  is fixed and positive definite, simply by solving for the zero gradient. Doing this for every row of  $A$  and summing up, we get that Problem 2 can be reduced to the following problem:

$$\max_k \sum_{c=1}^C y_c^\top (k + \mu I)^{-1} k y_c,$$

which is after writing the eigenvalue decomposition of  $K$  as  $VS^\top V^\top$  and using  $(k + \mu I)^{-1} k = V(S + \mu I)^{-1} V^\top V S V^\top$ , is equivalent to:

$$\max_k \sum_{c=1}^C \sum_{i=1}^{Cn} (y_c^\top v_i)^2 \frac{\lambda_i}{\lambda_i + \mu},$$

where  $\lambda_i, v_i$  are the  $i$ -th eigenvalue and eigenvector, respectively. By continuity of the Problem 2 in both variables, we can without loss of generality plug  $k^*$  into this despite being low-rank. This can be seen by contradiction – if the  $\mathcal{L}(A^*, k^*)$  would not be equal to  $\sum_{c=1}^C y_c^\top (k^* + \mu I)^{-1} k^* y_c$ , we can find a converging sequence  $k_i$  of symmetric PD kernel matrices that converges to  $k^*$  for which the two objectives are equal and by continuity they converge to the objectives evaluated at  $A^*, k^*$ , thus they must be equal as well. After a simple computation we get:

$$\mathcal{L}(A^*, k^*) = Cn \frac{n}{n + \mu}.$$

With slight abuse of notation let us now re-scale  $Y$ , so that each row is unit norm and divide the loss  $\mathcal{L}$  by  $C$ . Then we get (abusing the notation):

$$\mathcal{L}(A^*, k^*) = \frac{n}{n + \mu}.$$

Now,  $\sum_{i=1}^{Cn} (y_c^\top v_i)^2 = 1$  since  $(v_i)_{i=1}^{Cn}$  forms an orthogonal basis and therefore a tight frame with constant 1. Therefore the expression

$$\max_k \frac{1}{C} \sum_{c=1}^C \sum_{i=1}^{Cn} (y_c^\top v_i)^2 \frac{\lambda_i}{\lambda_i + \mu}$$

can be viewed as a weighted average of the  $\frac{\lambda_i}{\lambda_i + \mu}$  terms. To simplify the expression, denote  $\omega_i := \frac{1}{C} \sum_{c=1}^C (y_c^\top v_i)^2$ . Using Cauchy-Schwarz inequality on each individual summand, we see that  $(y_c^\top v_i)^2 \leq \sum_{j; y_{c_j}=1} v_{ij}^2$  and the equality is only achieved if all the entries of  $v_i$  corresponding to entries of  $y_c$  equal to 1 are the same. Thus, we get  $\sum_{c=1}^C (y_c^\top v_i)^2 \leq \|v_i\|^2 = 1$  with the equality if and only if, for each  $c$ , all the entries of  $q_i$  corresponding to the entries of  $y_c$  equal to 1 are the same. This gives that  $\omega_i \leq \frac{1}{C}$ .

Now, take any feasible  $k$ . Then,

$$\mathcal{L}(k, \alpha^*) = \sum_{i=1}^{Cn} \omega_i \frac{\lambda_i}{\lambda_i + \mu} \leq \frac{1}{C} \sum_{i=1}^C \frac{\lambda_i}{\lambda_i + \mu} < \frac{\frac{1}{C} \sum_{i=1}^C \lambda_i}{\frac{1}{C} \sum_{i=1}^C \lambda_i + \mu} \leq \frac{n}{n + \mu}.$$

The first inequality is due to the monotonicity of the function  $g(x) = \frac{x}{x + \mu}$  and  $\omega_i \leq \frac{1}{C}$ ; the second strict inequality is due to Jensen after noting that  $g$  is strictly convex and using the Perron-Frobenius theorem which says that  $\lambda_1$  has multiplicity 1; and the last inequality is due to  $\sum_{i=1}^{Cn} \lambda_i = Cn$ , which follows from the well-known trace inequality and the fact that  $k$  must have all the diagonal elements equal 1. This concludes the proof.  $\square$

### B.3 Random feature map separates the data

*Proof of Proposition A.1.* It can easily be seen that the separate indices  $(Wx, Wy)_{i=1}^D$  are i.i.d., therefore it suffices to analyze the  $\mathbb{E}(\sigma(w^T x)\sigma(w^T y))$  for a single row of  $W$ . For simplicity of computation, we will re-scale the  $w$  to have variance 1 entries and later re-scale back again. From the spherical symmetry of the multivariate standard normal distribution, we can without loss of generality assume that  $x = e_1 = (1, 0, \dots, 0)$  and  $y = re_1 + \sqrt{1-r^2}e_2 = (r, \sqrt{1-r^2}, 0, \dots, 0)$ . With this, the expectation reduces to  $\mathbb{E}(\sigma(w_1)\sigma(rw_1 + \sqrt{1-r^2}w_2))$ . We can further compute (while renaming  $x \equiv w_1; y \equiv w_2$ ):

$$\begin{aligned} \mathbb{E}(\sigma(w_1)\sigma(rw_1 + \sqrt{1-r^2}w_2)) &= \int_{\mathbb{R}} \int_{\mathbb{R}} \sigma(x)\sigma(rx + \sqrt{1-r^2}y) \frac{1}{2\pi} e^{-\frac{x^2}{2}} e^{-\frac{y^2}{2}} dx dy = \\ &= \sqrt{1-r^2} \int_{\mathbb{R}} \sigma(x) \frac{1}{\sqrt{2\pi}} e^{-\frac{x^2}{2}} \left( \int_{\mathbb{R}} \sigma\left(\frac{r}{\sqrt{1-r^2}}x + y\right) \frac{1}{\sqrt{2\pi}} e^{-\frac{y^2}{2}} dy \right) dx \end{aligned}$$

For the inner-integral, denote  $a = \frac{r}{\sqrt{1-r^2}}x$  for now. Then the inner integral can be computed as:

$$\int_{-a}^{\infty} (y+a) \frac{1}{\sqrt{2\pi}} e^{-\frac{y^2}{2}} dy = \int_{-a}^{\infty} y \frac{1}{\sqrt{2\pi}} e^{-\frac{y^2}{2}} dy + a \int_{-a}^{\infty} \frac{1}{\sqrt{2\pi}} e^{-\frac{y^2}{2}} dy = \frac{1}{\sqrt{2\pi}} e^{-\frac{a^2}{2}} + a\Phi(a),$$

where  $\phi(\cdot), \Phi(\cdot)$  will denote the pdf and cdf of the standard normal, respectively. Plugging back into the outer integral we get:

$$(\dots) = \sqrt{1-r^2} \int_0^{\infty} \frac{x}{2\pi} e^{-\frac{x^2}{2(1-r^2)}} dx + r \int_0^{\infty} \frac{x^2}{\sqrt{2\pi}} e^{-\frac{x^2}{2}} \Phi\left(\frac{rx}{\sqrt{1-r^2}}\right) dx.$$

We will compute the two summands separately:

$$\int_0^{\infty} \frac{x}{2\pi} e^{-\frac{x^2}{2(1-r^2)}} dx = \frac{\sqrt{1-r^2}}{\sqrt{2\pi}} \int_0^{\infty} \frac{x}{\sqrt{1-r^2}\sqrt{2\pi}} e^{-\frac{x^2}{2(1-r^2)}} dx = \frac{1-r^2}{2\pi},$$

where the last equality is a well-known formula for the expectation of ReLU of a Gaussian. For the second integral, denote  $a = \frac{r}{\sqrt{1-r^2}}$  and, using the integration by parts for  $x\phi(x)$  and  $x\Phi(ax)$  we can write

$$\begin{aligned} \int_0^{\infty} x^2 \phi(x) \Phi(ax) dx &= [-x\phi(x)\Phi(ax)]_0^{\infty} + \int_0^{\infty} \phi(x)\Phi(ax) dx + a \int_0^{\infty} x\phi(x)\phi(ax) dx \\ &= \int_0^{\infty} \phi(x)\Phi(ax) dx + a \int_0^{\infty} x\phi(x)\phi(ax) dx. \end{aligned}$$

The second integral evaluates to the same expression as the integral in the first summand above, but gets multiplied by  $a$  and thus equals  $\frac{r\sqrt{1-r^2}}{2\pi}$ . For the second integral, first note that this parametric integral is differentiable w.r.t.  $a$  and satisfies the condition on exchanging the derivative with the integral, so we will compute it using differentiation w.r.t.  $a$ . The value of the integral for  $a = 0$  is trivially  $1/4$ . After taking the derivative, it is easy to see that the integral evaluates to the same one we already computed twice, so denoting  $f(a) = \int_0^{\infty} \phi(x)\Phi(ax) dx$  we get

$$f'(a) = \frac{1}{2\pi(1+a^2)}.$$

We see that the  $f'$  is just half of the pdf of standard Cauchy distribution, while  $f(0)$  is half of its cdf, therefore  $f$  is half of its cdf and we can write:

$$f(a) = \frac{1}{4} + \frac{1}{2\pi} \arctan(a).$$

Plugging back the  $a$  and putting everything together we get the final:

$$\mathbb{E}(\sigma(w_1)\sigma(rw_1 + \sqrt{1-r^2}w_2)) = \frac{(1-r^2)^{\frac{3}{2}}}{2\pi} + \frac{r^2\sqrt{1-r^2}}{2\pi} + \frac{r}{4} + \frac{r}{2\pi} \arctan\left(\frac{r}{\sqrt{1-r^2}}\right).$$

We see that after scaling the weights with the scaling indicated in the statement, we get the final result. Since  $\sigma(w^T x)^T \sigma(w^T y)$  is clearly sub-exponential, the sum of  $D$  such i.i.d. variables will be as well.  $\square$



## C Experimental details

In both Deep RFM and neural networks, we one hot encode labels and use  $\pm 1$  for within/outside of each class.

For the neural network experiments, we use 5 hidden layer MLP networks with no biases and ReLU activation function. All experiments use SGD with batch size 128. We use default initialization for the linear readout layer. The layers all use width 512 in all experiments. All models are trained with MSE loss. We measure the AGOP and NC metrics every 10 epochs. VGG was trained for 600 epochs with 0.9 momentum, learning rate 0.01, and initialization 0.3 in the intermediate layers (0.2 for MNIST). ResNet was trained for 300 epochs, no momentum, 0.2 init. scale in the intermediate layers, and learning rate 0.05. MLPs were trained for 500 epochs, no momentum, 0.3 init. scale (0.2 for MNIST), and learning rate 0.05.

We use the standard ResNet18 architecture (from the Pytorch `torchvision` library), where we replace the classifier (a fully-connected network) at the end with 5 MLP layers (each layer containing a linear layer followed by a ReLU, without any biases). We truncate the VGG-11, as defined in `torchvision.models`, to the ReLU just before the final two pooling layers, so that the pooling sizes matches MNIST, which contains 28x28 images, then attach at the end a 5-layer MLP as the classifier.

For the Deep RFM experiments, we generally use the Laplace kernel  $k$ , which evaluates two datapoints  $x, z \in \mathbb{R}^d$  as  $k(x, z) = \exp(-\|x - z\|_2/L)$ , where  $L$  is a bandwidth parameter. For the experiments with ReLU on MNIST, we use the Gaussian kernel with bandwidth  $L$  instead. In these experiments, we set  $L = 2.0$ . We perform ridgeless regression to interpolate the data, i.e.  $\mu = 0$ . We use width 1024 for the random feature map in Deep RFM with ReLU activation function. For experiments with the cosine activation, we used Random Fourier Features corresponding to the  $\ell_1$ -Laplacian kernel with bandwidth  $\sigma = 0.05$  and 4096 total features.

Unless otherwise specified, we perform experiments using the first 50,000 points from each of MNIST, SVHN, and CIFAR-10 loaded with `torchvision` datasets.

For neural network experiments, we averaged over 3 seeds and report 1 standard deviation error bars, truncating the lower interval to  $0.01 \times$  the mean value. We report Pearson correlation for the NFA values (where each matrix is subtracted by its mean value). As noted in the main text, we compute correlation of the NFM with the square root of the AGOP as in Radhakrishnan et al. [2024a].

Each experiment was performed on a single NVIDIA A100 GPU. Each experiment was completed in under 1.5 GPU hours.

All code is available at this link: [https://anonymous.4open.science/r/neural\\_collapse\\_rfm-D792/](https://anonymous.4open.science/r/neural_collapse_rfm-D792/). See in particular `nc_nn.py` and `deep_rfm.py` for NN and Deep RFM code.

The code for Random Fourier Features (used in Deep RFM with cosine activation function) was adapted from <https://github.com/hichamjanati/srf.git>.

## D Additional plots

In this section, we give the full set of results for all combinations of datasets and neural network architectures for Deep RFM and standard DNNs (VGG, ResNet, and MLPs). In Figures 3 and 5, we plot the NC1 and NC2 metrics for Deep RFM as a function of the layer for ReLU and cos activation functions. In Figures 4 and 6, we visualize the formation of DNC in Deep RFM as in the main text. In Figures 7, 8, and 9, we demonstrate that the right singular structure can reduce the majority of NC1 reduction in MLPs, ResNet, and VGG, respectively. In Figures 10, 11, and 12, we verify the NFA, DNC, and plot the training loss.

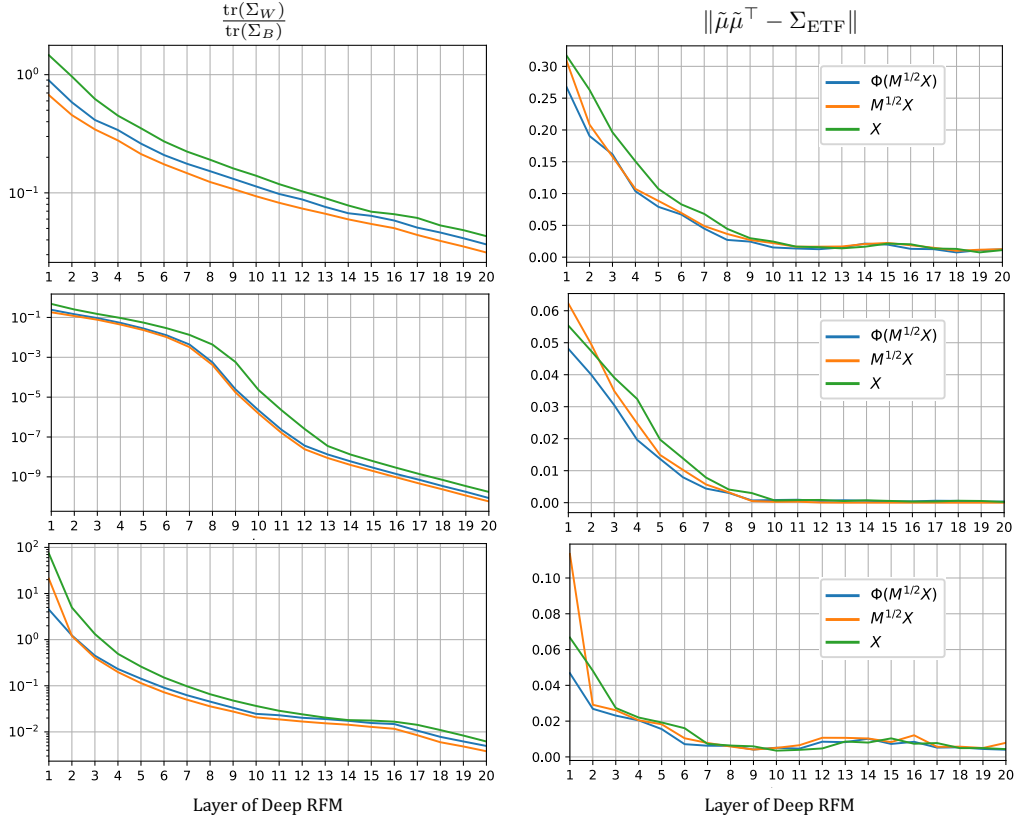


Figure 3: Neural collapse with Deep RFM on additional datasets with  $\sigma(\cdot) = \text{ReLU}(\cdot)$ . We show  $\text{tr} \Sigma_W / \text{tr} \Sigma_B$ , our NC1 metric on the left, and  $\|\tilde{\mu}\tilde{\mu}^\top - \Sigma_{\text{ETF}}\|$ , our NC2 metric, on the right. The first row is CIFAR-10, second is MNIST, third is SVHN. We plot these metrics as a function of depth of Deep RFM for the original data  $X$  (green), the data after applying the square root of the AGOP  $M^{1/2}x$  (orange), and the data after the AGOP and non-linearity (blue).

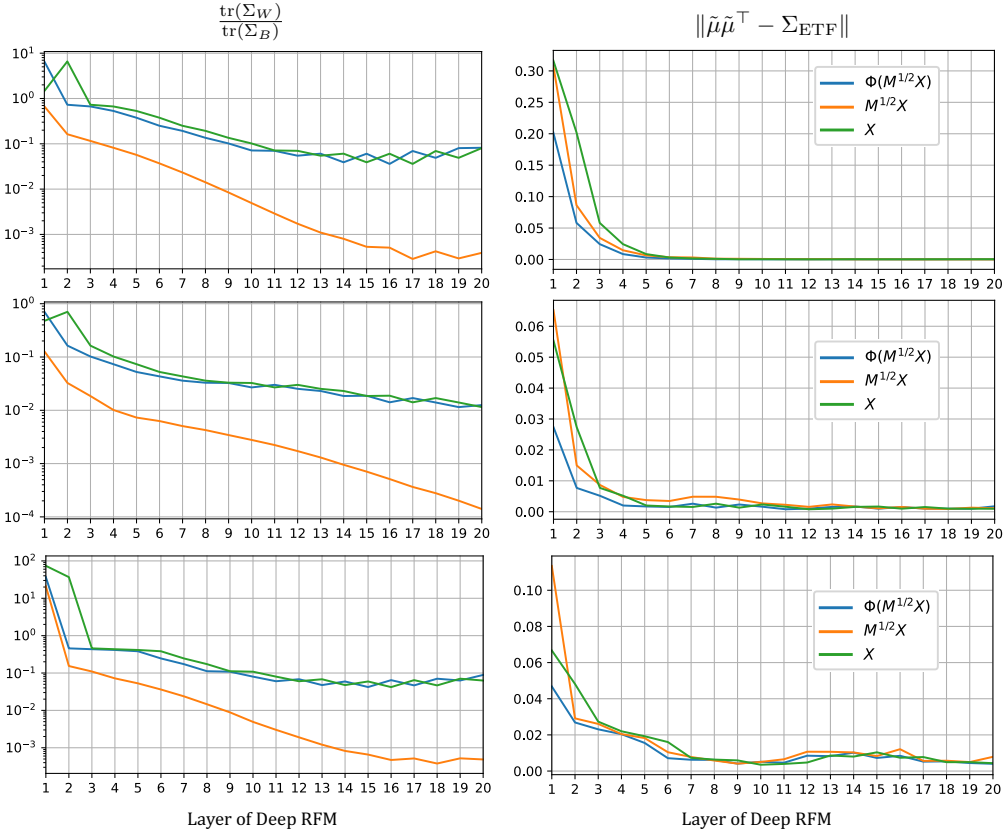


Figure 4: Neural collapse with Deep RFM on additional datasets with  $\sigma(\cdot) = \cos(\cdot)$ . We show  $\text{tr} \Sigma_W / \text{tr} \Sigma_B$ , our NC1 metric on the left, and  $\|\tilde{\mu}\tilde{\mu}^\top - \Sigma_{\text{ETF}}\|$ , our NC2 metric, on the right. The first row is CIFAR-10, second is MNIST, third is SVHN. We plot these metrics as a function of depth of Deep RFM for the original data  $X$  (green), the data after applying the square root of the AGOP  $M^{1/2}x$  (orange), and the data after the AGOP and non-linearity (blue).

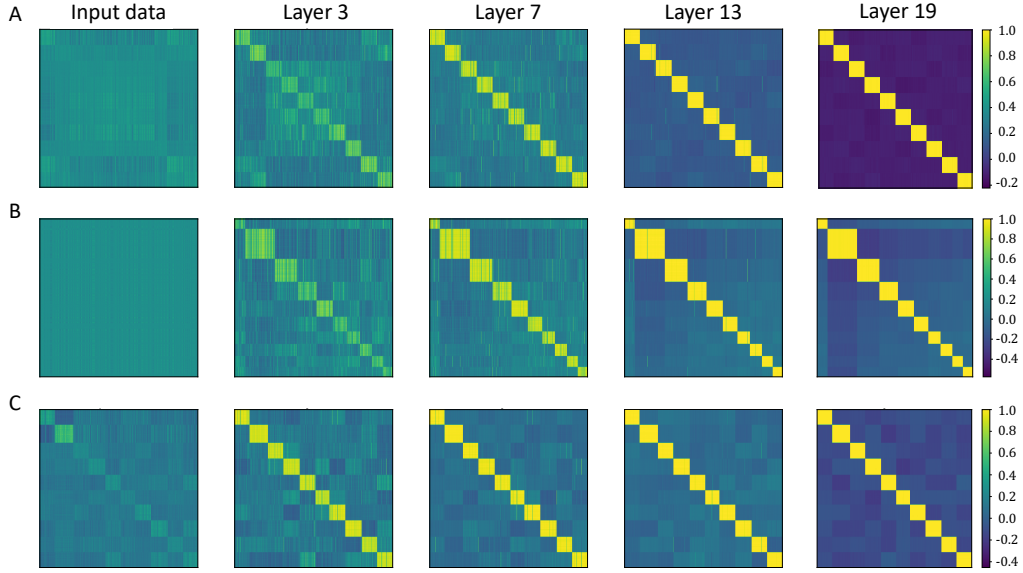


Figure 5: Visualization of neural collapse for Deep RFM on additional datasets with  $\sigma(\cdot) = \cos(\cdot)$ . As in the main text, we plot the gram matrix of the feature vectors after applying  $M^{1/2}$ , where the data are ordered by class. We see the data form the ETF in the final column. (A) corresponds to CIFAR-10, (B) SVHN, and (C) MNIST.

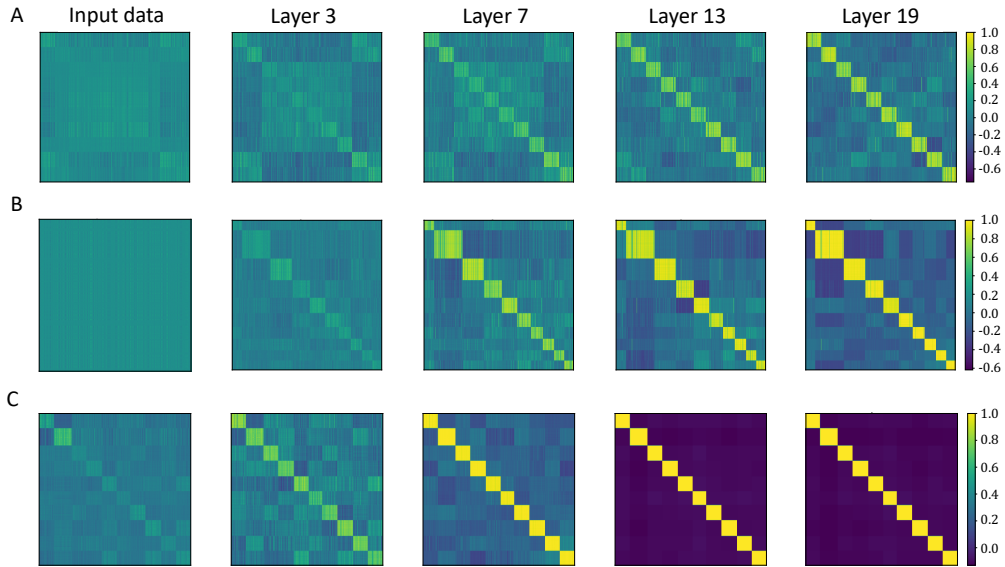


Figure 6: Visualization of neural collapse for Deep RFM on additional datasets with  $\sigma(\cdot) = \text{ReLU}(\cdot)$ . As in the main text, we plot the gram matrix of the feature vectors after applying  $M^{1/2}$ , where the data are ordered by class. We see the data form the ETF in the final column. (A) corresponds to CIFAR-10, (B) SVHN, and (C) MNIST.

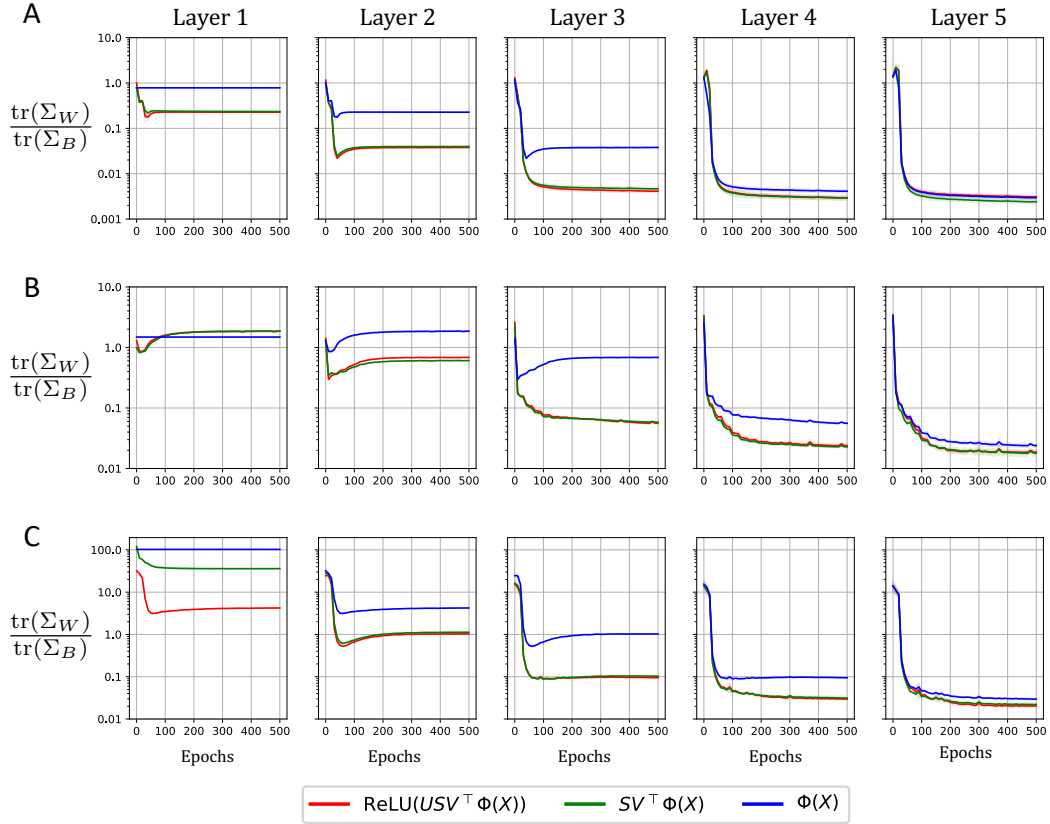


Figure 7: Feature variability collapse (NC1) from different singular value decomposition components on an MLP. The first row (A) is MNIST, second (B) is CIFAR-10, third (C) is SVHN. As in the main text, we plot the NC1 metrics, for the original feature vectors  $\Phi(X)$  (blue), the data after applying the right singular structure (green), and the data after the full layer application (red).

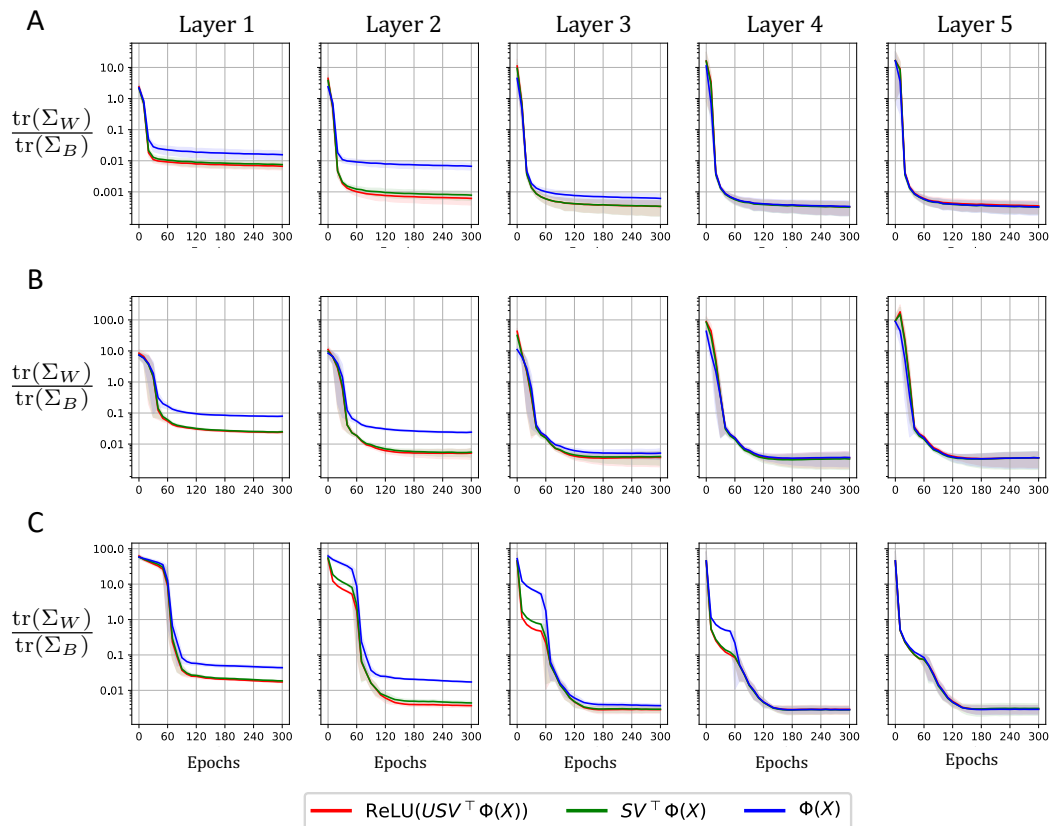


Figure 8: Feature variability collapse (NC1) from different singular value decomposition components on ResNet. The first row (A) is MNIST, second (B) is CIFAR-10, third (C) is SVHN. As in the main text, we plot the NC1 metrics, for the original feature vectors  $\Phi(X)$  (blue), the data after applying the right singular structure (green), and the data after the full layer application (red).

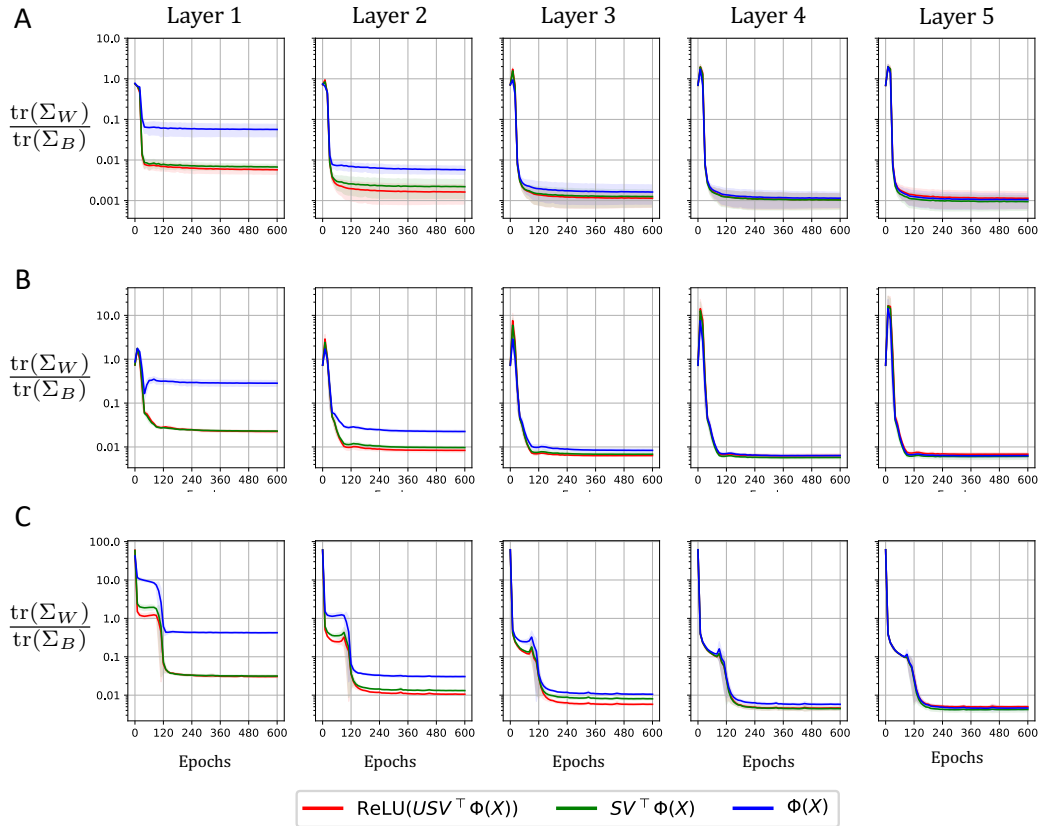


Figure 9: Feature variability collapse (NC1) from different singular value decomposition components on VGG. The first row (A) is MNIST, second (B) is CIFAR-10, third (C) is SVHN. As in the main text, we plot the NC1 metrics, for the original feature vectors  $\Phi(X)$  (blue), the data after applying the right singular structure (green), and the data after the full layer application (red).

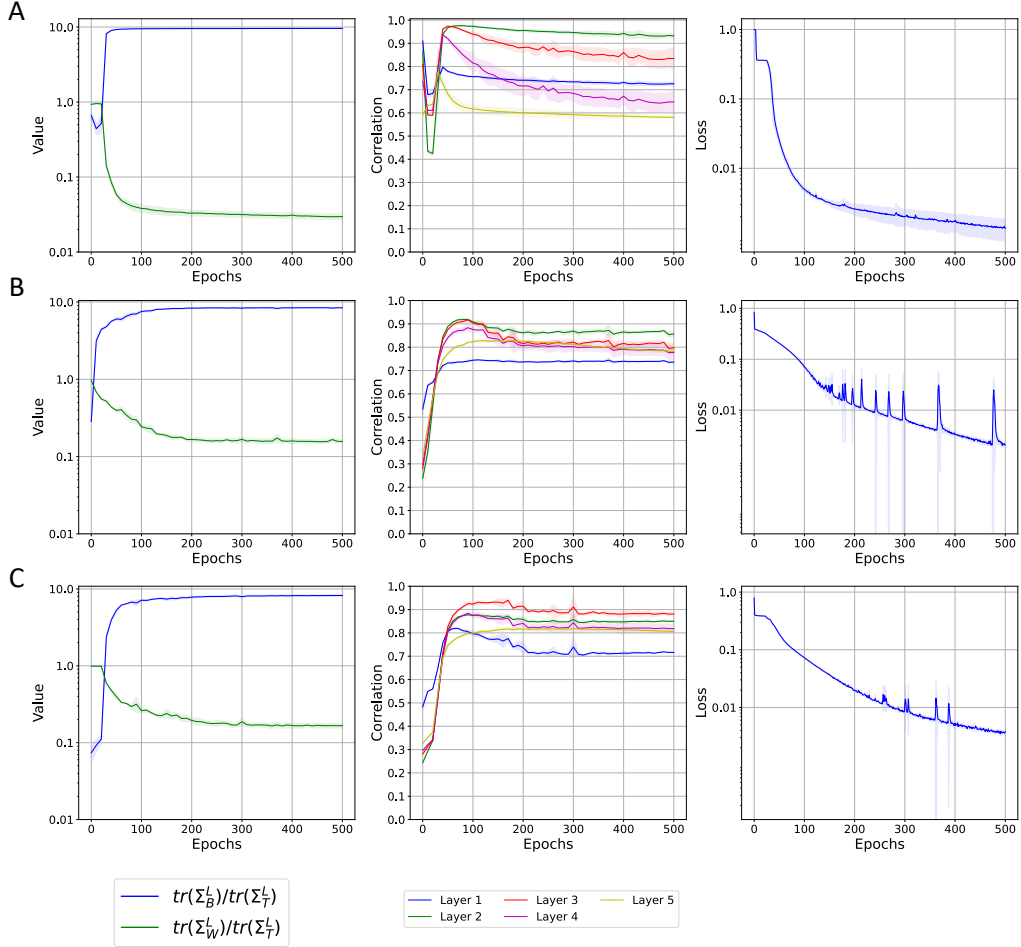


Figure 10: Train loss and NFA correlations for MLPs. The first row (A) is MNIST, second (B) is CIFAR-10, third (C) is SVHN. In the first column, we plot the evolution of  $\text{tr} \Sigma_W / \text{tr} \Sigma_T$  and  $\text{tr} \Sigma_B / \text{tr} \Sigma_T$ , where  $\Sigma_T \triangleq \Sigma_W + \Sigma_B$ . In the second column we plot the development of the NFA, where correlation is measured between  $W_l^T W_l$  and the square root of the AGOP with respect to the inputs at layer  $l$ ,  $X_l$ . The third column is the train loss of the neural network.



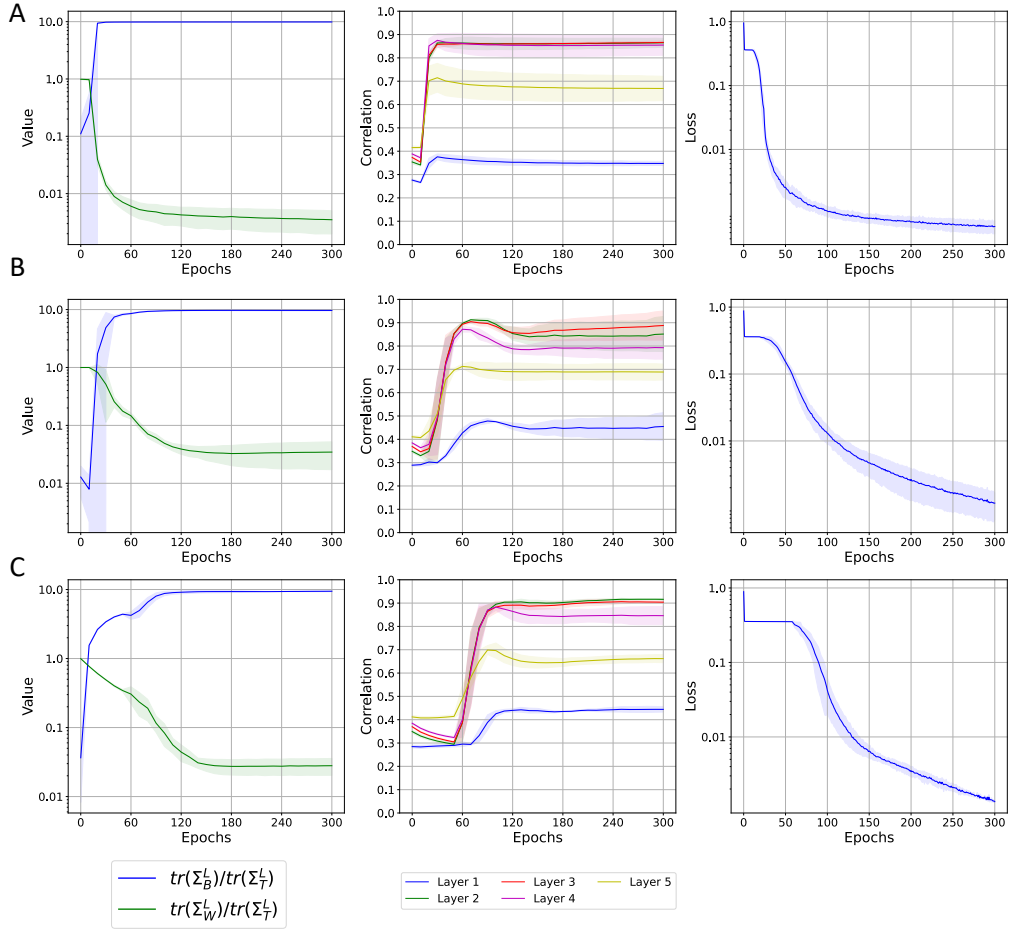


Figure 11: Train loss and NFA correlations for ResNet. The first row (A) is MNIST, second (B) is CIFAR-10, third (C) is SVHN. In the first column, we plot the evolution of  $\text{tr} \Sigma_W / \text{tr} \Sigma_T$  and  $\text{tr} \Sigma_B / \text{tr} \Sigma_T$ , where  $\Sigma_T \triangleq \Sigma_W + \Sigma_B$ . In the second column we plot the development of the NFA, where correlation is measured between  $W_l^T W_l$  and the square root of the AGOP with respect to the inputs at layer  $l$ ,  $X_l$ . The third column is the train loss of the neural network.

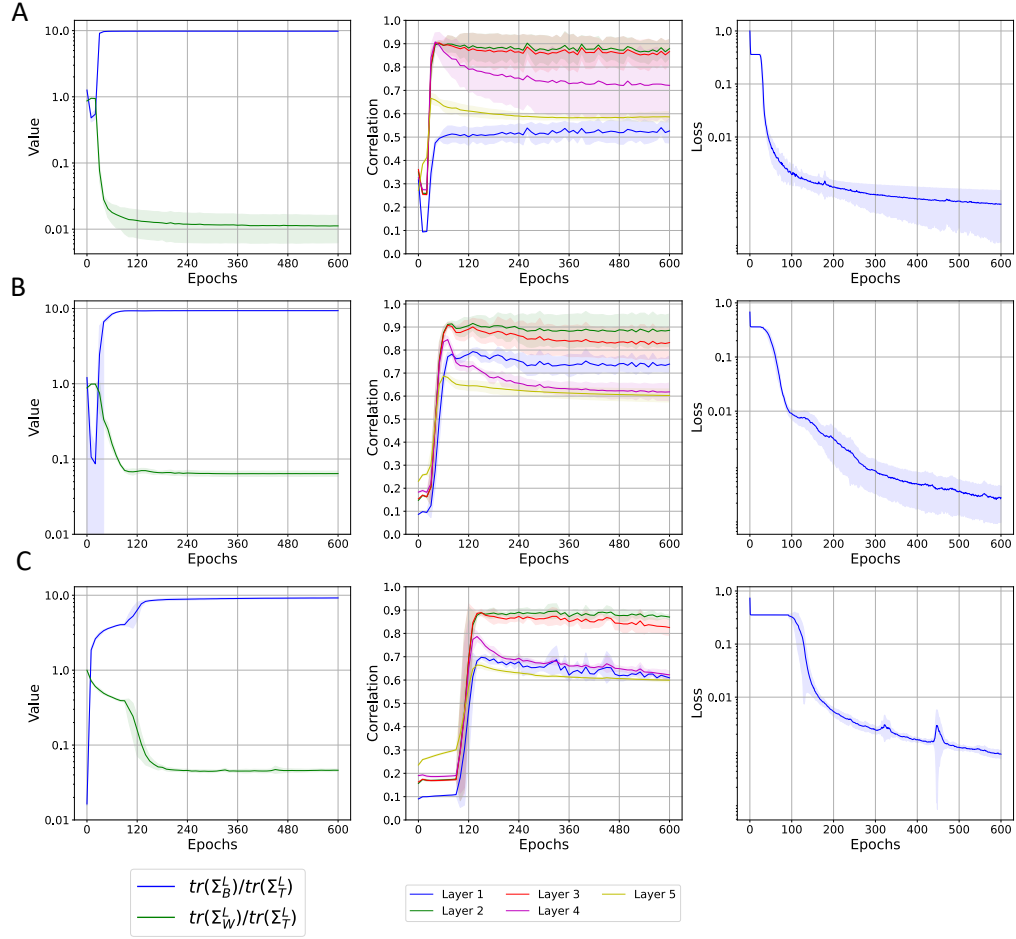


Figure 12: Train loss and NFA correlations for VGG. The first row (A) is MNIST, second (B) is CIFAR-10, third (C) is SVHN. In the first column, we plot the evolution of  $\text{tr} \Sigma_W / \text{tr} \Sigma_T$  and  $\text{tr} \Sigma_B / \text{tr} \Sigma_T$ , where  $\Sigma_T \triangleq \Sigma_W + \Sigma_B$ . In the second column we plot the development of the NFA, where correlation is measured between  $W_l^\top W_l$  and the square root of the AGOP with respect to the inputs at layer  $l$ ,  $X_l$ . The third column is the train loss of the neural network.